

# Dynamic Pressure Sensitive Paint Demonstration in the AEDC Propulsion Wind Tunnel 16T\*

Marvin E. Sellers<sup>1</sup> and Michael A. Nelson<sup>2</sup>  
*Aerospace Testing Alliance, Arnold AFB, TN, 37389*

Jim W. Crafton<sup>3</sup>  
*Innovative Scientific Solutions, Inc., Dayton, OH, 45459*

Unsteady aerodynamics has been difficult to measure since the beginning days of wind tunnel testing. Distributed dynamic loads have been determined by using special (dynamic) transducers that measure pressure fluctuations at a few to several hundred points on a wind tunnel model and then integrating the pressure fluctuations over a specified area. Typical data acquisition systems that capture the pressure fluctuations record at rates up to 50,000 samples/channel/second and can generate many terabytes of raw data. Processing the large amount of data generated typically cannot be accomplished during wind tunnel tests, so selected data are processed for evaluation during testing. Another area of concern over the last several decades has been weapons bay acoustics and their effect on store separation. The U.S. Air Force (USAF) needs to understand the aerodynamics of payloads separating from aircraft to support weapons system design and certification. Customers to the Air Force such as Lockheed Martin Aeronautics Company have been developing computational fluid dynamics (CFD) models of stores separation in order to reduce the amount of wind tunnel and flight testing required for the certification process on each weapon and platform. Currently CFD validation can only be performed at point locations where dynamic pressure transducers are installed. Engineers at the Arnold Engineering Development Complex (AEDC) have utilized a steady-state pressure-sensitive paint (PSP) capability in the Propulsion Wind Tunnel (PWT) 16T to acquire surface pressure data on wind tunnel models. A logical next step was to extend this capability to measure fluctuating pressures with PSP. Innovative Scientific Solutions, Inc. (ISSI) has developed a fast-responding PSP under USAF and NASA Phase II small business innovation research (SBIR) grants that can detect pressure fluctuations up to 20kHz. This was made possible by new developments in high-speed camera technology and brighter light emitting diode (LED) technology. However, the test section in 16T places the test article approximately 8-11 feet away from cameras and LEDs. Detecting the fluorescence emitted by the fast PSP with exposure times in the hundreds of micro-seconds would be a challenge. In support of the Air-Delivered Weapon Certification Cost Reduction program, ISSI was awarded a grant to demonstrate the fast PSP capability in 16T with AEDC and Lockheed as partners. ISSI would provide the technical assistance, equipment and PSP, Lockheed would perform CFD computations and provide the test article, and AEDC would develop data acquisition and image processing software and perform the wind tunnel testing in 16T. Power spectral density (PSD) comparisons are made between the fast PSP and conventional dynamic pressure transducers. In addition, the complete spatial distribution of the sound pressure level (SPL) at selected frequencies are presented to aid understanding of the data and provide additional insight. Proper Orthogonal Decomposition is applied to the data for identification of relevant flow structures.

---

\* The research reported herein was performed by the Arnold Engineering Development Complex (AEDC), Air Force Materiel Command. Work and analysis for this research were performed by personnel of Aerospace Testing Alliance, the operations, maintenance, information management, and support contractor for AEDC. Further reproduction is authorized to satisfy needs of the U. S. Government.

<sup>1</sup>AEDC Fellow, Integrated Test & Evaluation, Flight Systems, 740 Fourth St, MS6001.

<sup>2</sup>PSP Engineer, Integrated Test & Evaluation, Flight Systems, 740 Fourth St, MS6001

<sup>3</sup>Research Scientist, Innovative Scientific Solutions, Inc. 7610 McEwen Rd., AIAA Senior Member.

This paper is declared a work of the U.S. government and not subject to copyright protection in the United States.

## Nomenclature

$a_n$	=	Time constant
$A$	=	Eigenvectors of the correlation matrix
Alpha	=	Model angle of attack, deg
Beta	=	Model sideslip angle, deg
B.L.	=	Model buttock line, model scale in.
$\bar{C}$	=	Correlation matrix
CONFIG	=	Configuration designation number
CP	=	Surface pressure coefficient, $(P - P_\infty) / Q_\infty$
D	=	Diffusion coefficient
f	=	Frequency, Hz
FFT	=	Fast-Fourier Transform
FIB7	=	Proprietary polymer developed by the University of Washington
F.S.	=	Model fuselage station, model scale in.
h	=	Paint thickness
$\lambda$	=	Eigenvalues of the correlation matrix
l/d	=	Cavity length over depth ratio
$I$	=	Paint luminescence intensity at pressure
$IR$	=	Intensity ratio
LED	=	Light-emitting diode
Mach, M	=	Free-stream Mach number
$\Phi$	=	POD mode
$P$	=	Pressure at wind-on condition, psfa
PSD	=	Power spectral density, $\text{psi}^2/\text{Hz}$
PSP	=	Pressure-sensitive paint
r	=	Temperature recovery factor [see Eq. (5)]
SPL	=	Sound pressure level, dB
t	=	Time, s
$\tau_{\text{diff}}$	=	Diffusion response time constant
$T_{\text{surface}}$	=	PSP calibration or model surface temperature, °F
$T_\infty$	=	Freestream temperature, °F
$TT$	=	Tunnel stagnation temperature, °F
u	=	Column vector of spatial pressure distribution at time t, psf
U	=	Group of snapshots (u) of pressure distribution, psf
W.L.	=	Model water line, model scale in.

## I. Introduction

UNSTEADY aerodynamics has been difficult to measure since the beginning days of wind tunnel testing. Total vehicle dynamics have been captured using specially designed "dynamic" balances to measure damping forces. Distributed dynamic loads have been determined by using special (dynamic) transducers that measure pressure fluctuations at a few to several hundred points on a wind tunnel model and then integrating the pressure fluctuations over a specified area. Typical data acquisition systems that capture the pressure fluctuations record at rates up to 50,000 samples/channel/second and can generate many terabytes of raw data. Processing the large amount of data generated typically cannot be accomplished during wind tunnel tests, so selected data are processed for evaluation during testing. Another area of concern over the last several decades has been weapons bay acoustics and their effect on store separation. The U.S. Air Force (USAF) needs to understand the aerodynamics of payloads separating from aircraft to support weapons system design and certification. Customers to the Air Force such as Lockheed Martin Aeronautics Company have been developing computational fluid dynamics (CFD) models of stores separation in order to reduce the amount of wind tunnel and flight testing required for the certification process on each weapon and platform. Currently CFD validation can only be performed at point locations where dynamic pressure transducers are installed.

Engineers at the Arnold Engineering Development Complex (AEDC) have utilized a steady-state pressure-sensitive paint (PSP) capability in the Propulsion Wind Tunnel (PWT) 16T to acquire surface pressure data on wind tunnel models (Refs. 1 through 9). The technique uses a special paint that fluoresces with an intensity that is inversely proportional to the surface pressure, i.e., low pressure is brighter than high pressure. Some advantages of using PSP are: 1) it provides a significantly more complete pressure distribution than is possible with individual pressure orifices, 2) it permits the acquisition of data in areas inaccessible to conventional pressure measurements and 3) provides data mapped to a 3-D surface grid similar to CFD permitting better validation of CFD results. In addition, PSP data can easily be integrated over individual surfaces to determine panel loads. The PSP data acquisition system is controlled by the facility computer for automation and can provide engineering unit data within 10 seconds of acquisition.

A logical next step was to extend this capability to measure fluctuating pressures with PSP. Innovative Scientific Solutions, Inc. (ISSI) has developed a fast-responding PSP under USAF and NASA Phase II small business innovation research (SBIR) grants that can detect pressure fluctuations up to 20kHz. The capability to measure fluctuating pressures with a fast (or dynamic) PSP has been demonstrated by ISSI in several small research facilities (Ref. 10). This was made possible by new developments in high-speed camera technology and brighter light emitting diode (LED) technology. However, the test section in 16T places the test article approximately 8-11 feet away from cameras and LEDs. Detecting the fluorescence emitted by the fast PSP with exposure times in the hundreds of micro-seconds would be a challenge. In support of the Air-Delivered Weapon Certification Cost Reduction program, ISSI was awarded a grant to demonstrate the fast PSP capability in 16T with AEDC and Lockheed as partners. ISSI would provide the technical assistance, equipment and PSP, Lockheed would perform CFD computations and provide the test article, and AEDC would develop data acquisition and image processing software and perform the wind tunnel testing in 16T. Power spectral density (PSD) comparisons are made between the fast PSP and conventional dynamic pressure transducers. In addition, the complete spatial distribution of the sound pressure level (SPL) at selected frequencies are presented to aid understanding of the data and provide additional insight. Proper Orthogonal Decomposition is applied to the data for identification of relevant flow structures.

## II. Background

### A. Pressure-Sensitive Paint Theory

PSP measurement systems exploit the sensitivity of certain luminescent molecules to oxygen density through the phenomenon of oxygen quenching. In a typical luminescent molecule, excitation by capture of a high-energy photon is followed by emission of a lower energy photon. As a result, the emitted photon will have a longer wavelength than the original exciting photon. The shift in emission wavelength from the absorption wavelength permits the measurement of emission intensity, or luminescence, with the use of appropriate filters. An alternate transition to the ground state is provided by collision with an oxygen molecule. Rather than emitting a photon, the excess energy of the luminescent molecule is absorbed by the oxygen molecule (oxygen quenching) during a collisional deactivation. Increasing amounts of oxygen increase the collisional deactivations, resulting in a decrease in the amount of luminescence. Since the number of oxygen molecules is directly proportional to the local pressure, low-pressure regions on the surface of a model will be brighter than regions of high pressure.

Two techniques exist for measurement of steady-state surface pressure using PSP; one is the "intensity" technique, and the other is the "lifetime" technique. In 2001, AEDC changed from the intensity technique (wind-off image / wind-on image) to the lifetime technique to overcome limitations of the intensity method, primarily model perspective change to the camera between wind-off and wind-on images when using pitch-roll to set Alpha-Beta angles. As indicated by the name, the "intensity" technique measures the paint fluorescence during the exposure and under constant illumination. The "lifetime" technique measures the paint fluorescence, under pulsed illumination, at two points in the lifetime response; one image during the excitation pulse and a second after the pulse during the fluorescence decay. A detailed description of the "intensity" technique can be found in Refs. 1-5 and the "lifetime" technique in Refs. 6-9. While there are limitations with the intensity technique, the dynamic PSP data are acquired in this mode (constant illumination) with high speed cameras capturing intensity fluctuations which are representative of pressure fluctuations.

## B. Pressure-Sensitive Paint

Two layers of paint are typically applied to the model surface. The first is a white substrate that helps reflect the luminescent light away from the model surface and provides a uniform background. For steady-state PSP, the first layer consists of the proprietary FIB7 polymer, developed by the University of Washington, with Titanium Dioxide. The second, the PSP layer, contains the FIB7 polymer and the luminescent molecule Platinum Tetra Pentafluorophenyl Porphine (PtTFPP), which is the active probe. The FIB7 polymer is porous to oxygen molecules, permitting contact with the PtTFPP molecules. One advantage of the FIB7 PSP is the low temperature sensitivity. However, the response to pressure fluctuations is limited by the diffusion of oxygen in the binder with response times on the order of 1 second. Frequency content up to 2,000 Hz are expected in the weapons bay cavity which eliminates FIB7 as a candidate. A fast-responding PSP formulation similar to those utilized by Gregory (see Ref. 11) is required for this test.

The temporal-response characteristics of PSP are primarily governed by the thickness of the paint formulation and the diffusion coefficient of the binder material, according to the relation

$$\tau_{diff} \propto \frac{h^2}{D_m} \quad (1)$$

where the response time due to diffusion ( $\tau_{diff}$ ) increases with the paint thickness ( $h$ ) squared and decreases with increasing diffusion coefficient ( $D_m$ ). Some investigators have focused on decreasing the thickness of the paint in order to improve the response characteristics. This approach, however, has the disadvantage of sacrificing luminescent output from the paint and, thus, the signal-to-noise ratio (SNR). The paint formulation used in this demonstration is developed based on the strategy of increasing the diffusivity of gas within the paint binder. Porous binders have been developed with the goal of enhancing the oxygen diffusion within the paint layer and, thus, improving the temporal response characteristics.

The difference between a conventional polymer-based PSP and a porous PSP is described schematically in Fig. 1. For conventional PSP, oxygen molecules in a test gas must permeate into the binder layer for oxygen quenching. The process of oxygen permeation in a polymer binder layer produces slow response times for a conventional PSP. On the other hand, the dye in a porous PSP is opened to the test gas so that the oxygen molecules are free to interact with the dye. The open binder creates a PSP that responds much more quickly to changes in oxygen concentration and, thus, pressure. A large effective surface area due to the porous surface improves luminescence intensity; thus, a higher SNR can be achieved. The drawback of the porous PSP approach is that the dye is too accessible to the oxygen. This results in near-complete quenching of all of the dye molecules at very high pressures. i.e. near atmosphere. These formulations are more effective at sub-atmospheric conditions. For low speed applications, the SNR suffers.

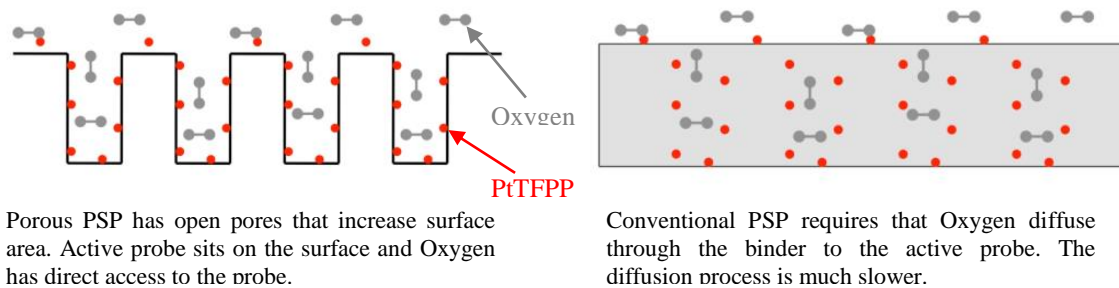


**Figure 1. Comparison of Porous PSP and Conventional PSP.**

Polymer/ceramic PSP has been developed as a hybrid paint formulation that incorporates the advantages of both traditional and porous PSP. The resulting system is a fast-time-response paint layer with favorable SNR at higher pressure, and the paint can be sprayed onto a model. The polymer/ceramic formulation incorporates a high percentage of ceramic particles that provide the porous structure for rapid oxygen quenching, with a small amount of polymer to bind the paint to the surface. A dye molecule with a short lifetime, such as PtTFPP, was deposited onto the polymer/ceramic surface to complete the paint formulation for this test. The absorption and emission spectral characteristics of PtTFPP in FIB7 and the excitation source are presented in Fig. 2. Each spectrum was normalized by its peak output. The polymer/ceramic (PC) PSP with PtTFPP has similar spectral characteristics.

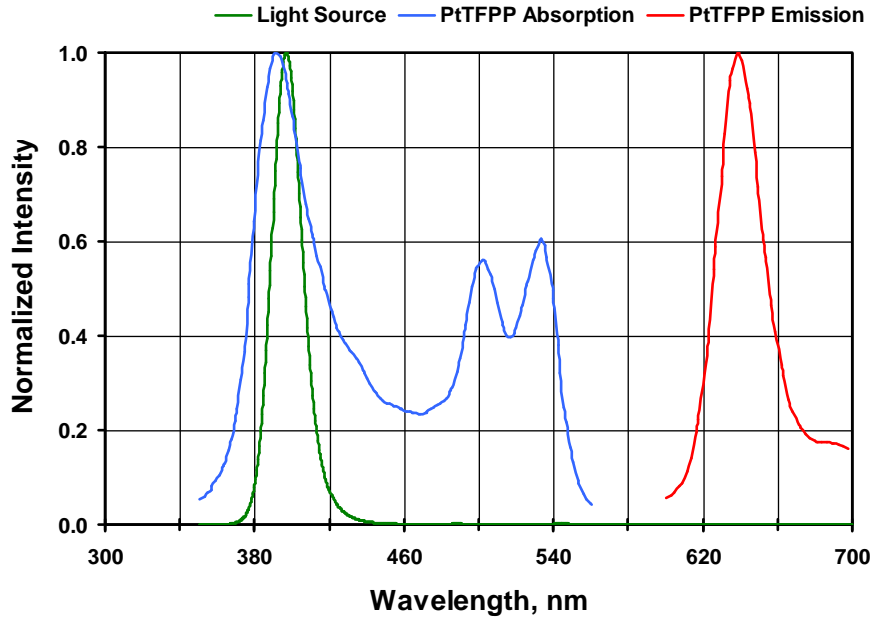


Figure 2. Spectral Characteristics of PtTFPP in FIB7 and Filtered Light Source.

### III. Test Setup

#### A. Test Article

The test article was a 1/15th scale model of an advanced tactical fighter concept vehicle with a generic weapons bay for the specific purpose of evaluating bay cavity flow. The bay opening was 11" inches long and 4.13" wide with a depth of 1.78" for the majority of the bay and decreasing to 0.94" (over 2.73" length) at the front wall. The cavity has an effective length-to-depth ratio of 6.18. The inlets were a flow-through design with blocking plates that could attach to the model base to provide 30% and 100% blockage. The model was mounted inverted on a strut. The bay was instrumented with 13 Kulite® dynamic pressure transducers and 19 static surface pressure orifices. The static pressures were connected to an Electronically Scanned Pressure (ESP) module. The Kulites® were connected to the dynamic data acquisition system (DDAS). The test article installation is presented in Fig. 3 with the paint fluorescence captured in the right photo. Details of the test article are presented in Fig. 4 along with pictorial location and designation of the dynamic transducer locations.

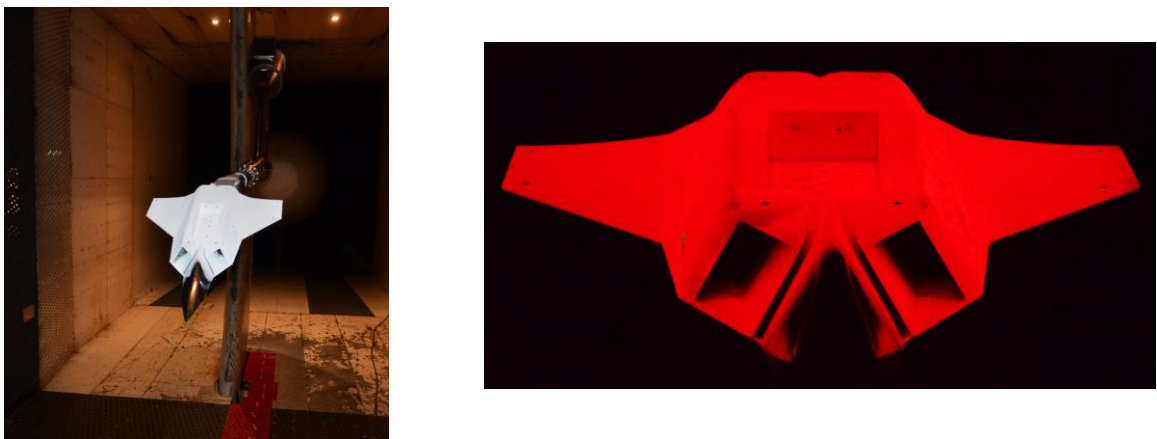
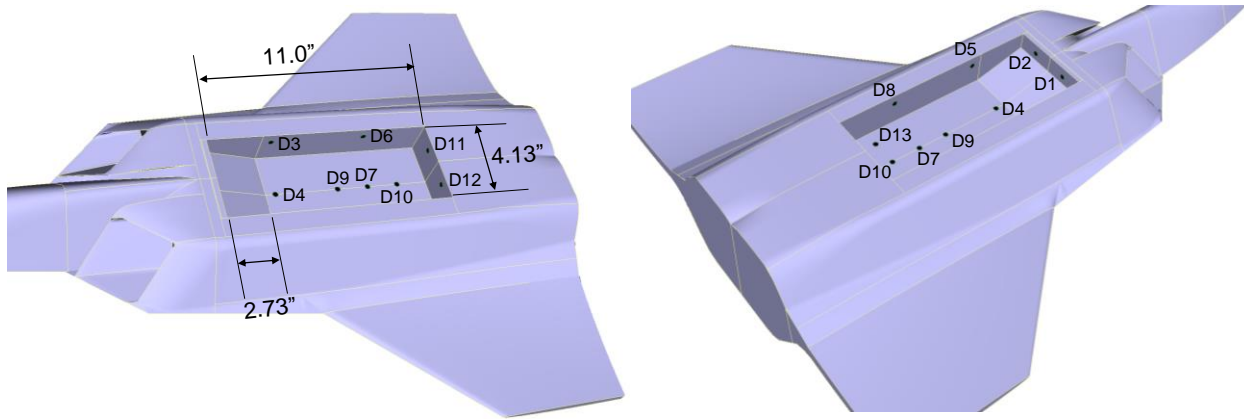


Figure 3. Test Article Installation.



**Figure 4. Test Article Details.**

### B. Dynamic Pressure-Sensitive Paint Data Acquisition System

The dynamic PSP data acquisition system (DPSPDAS) utilized some of the steady-state PSP system hardware. A schematic of the DPSPDAS is presented in Fig 5. The paint was excited by 30 light-emitting diode (LED) units, 10 LEDs per wall (top and sides), which illuminate at a wavelength of 396 nm. The LEDs operate in a pulsed mode for the steady-state PSP with a 5-percent duty cycle. New power supplies were provided by ISSI to operate the LEDs in DC mode (continuous output) but were limited to tens of seconds light output to avoid damaging the LEDs. The PSP luminescence was measured with two Vision Research Phantom® v711 high-speed cameras. Each camera has a 1200x800 pixel CMOS chip capable of recording full-frame images up to 7,500 frames/second. The chip is monochrome with 12-bit resolution. The luminescent light emitted by the paint was passed to the camera detector through a custom narrow-bandpass filter with a pass band of 570 to 700 nm. A Berkley Nucleonics Corporation (BNC) 555 digital delay generator turned on the LEDs and started camera acquisition. The two Phantom® cameras were synched to acquire images simultaneously and were framed by internal clocking once the external trigger to start was received. The LEDs were turned on 0.5 seconds prior to starting image acquisition. A Linux server class computer executed the data acquisition software that controlled the delay generator and cameras. The cameras were connected via fiber optic cable to a dual 10Gb Ethernet card. A supply of pressurized air was used to cool the PSP equipment since it was exposed to the low-pressure environment in the tunnel plenum area.

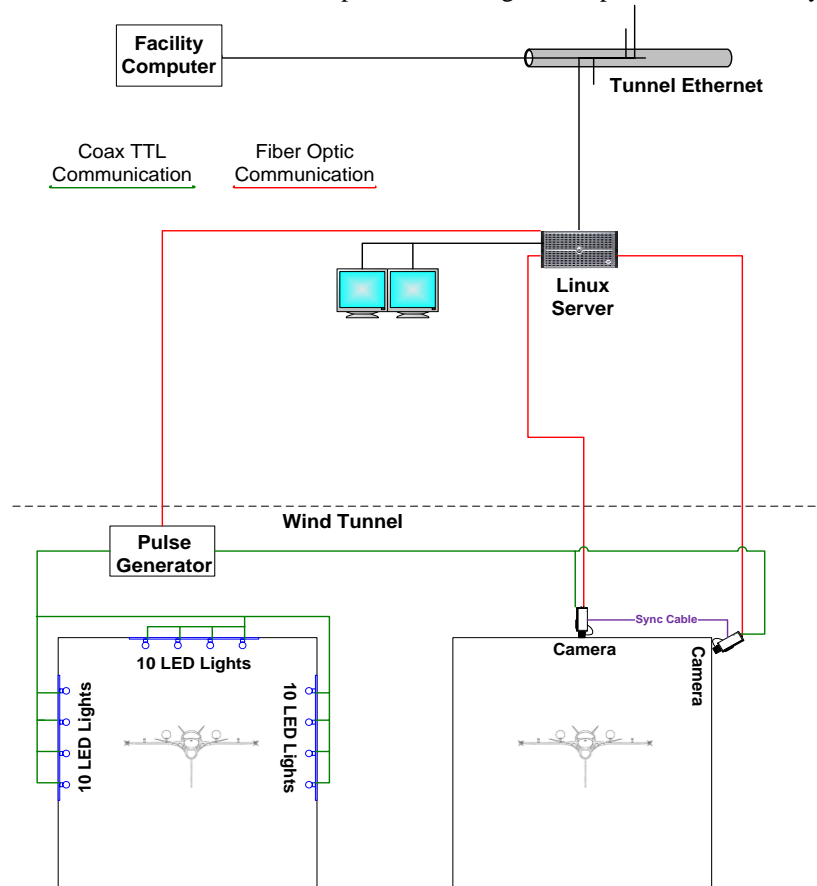


**Figure 5. Dynamic PSP Data Acquisition System.**

trigger to start was received. The LEDs were turned on 0.5 seconds prior to starting image acquisition. A Linux server class computer executed the data acquisition software that controlled the delay generator and cameras. The cameras were connected via fiber optic cable to a dual 10Gb Ethernet card. A supply of pressurized air was used to cool the PSP equipment since it was exposed to the low-pressure environment in the tunnel plenum area.

### C. Data Acquisition Procedures

Conventional steady-state and dynamic pressure data were acquired automatically by the facility data acquisition systems. The facility computer set the requested model attitude and sent the run and sequence number to the DPSPDAS, indicating that PSP data were to be acquired while the facility systems acquired the conventional pressure data. The conventional dynamic pressure data were acquired by the DDAS at 15,000 samples/sec for 10 second duration. The DPSPDAS started the pulse generator, which turned the LEDs on and 0.5 seconds later triggered the Phantom® cameras to start image acquisition. Image data were acquired at 2000, 3000, or 4000 frames/sec for 4.1 sec, 1.37 sec, and 4.1 sec, respectively. The exposure times were 495 μs, 325 μs, and 245 μs for the three data rates. The image data were stored locally in each camera and then downloaded to the server. A file containing tunnel conditions and conventional steady-state pressure data was generated for each data point and stored on the DPSPDAS. The conventional dynamic pressure data was stored locally on the DDAS. The DPSPDAS returned a code to the facility computer once data acquisition and storage was completed so the facility could advance to the next attitude or test condition.

Dynamic PSP data were acquired with the flow-through ducts 100% open and 100% blocked at Mach 0.9 and 1.3 for angles of attack -2, 0 and 5 degrees and sideslip angles of 0 and 2 degrees. The Reynolds number was constant at 2.0 million per foot, except for two data points (one for each configuration) at Mach 0.9 and 2.5 million per foot.

### D. Pressure-Sensitive Paint Data Reduction

The conversion of intensity images to surface pressure are proprietary, however, many of the steps that are applied to steady-state PSP (Refs. 1-9) also apply to dynamic PSP. Registration targets were applied to the model, and their positions in model coordinates were measured using a portable coordinate-measuring machine (CMM). The registration targets were used to relate the two-dimensional (2D) image coordinate system to the three-dimensional (3D) model coordinate system. The photogrammetry methods described by Bell (Ref. 12) and Ruyten (Ref. 13) were used to overlay the 2D pressure distribution from each camera onto a 3D mesh grid of the model surface. For each vertex point in the grid, a 7 by 7 average of the pressure was extracted from the 2D image. If a vertex point was visible to more than one camera, the pressure data were averaged using a weighting factor that was a function of the camera viewing angle. A 3D time history file was generated for each data point with pressure data, in psi, at each vertex point in the grid.

Comparisons of time history data between the dynamic pressure transducers and PSP is not possible since they were recorded at different sample rates and by systems not synchronized in time. However, comparisons of data in the frequency domain can be made. Since the dynamic pressure transducers were sampled at a faster rate than the PSP, the transducer data were down-sampled to the same rate as the PSP data and the PSDs were calculated. The two sets of data were processed identically (but on different systems) to produce the PSD data. The PSD was calculated using an ensemble size of 1024, with 50% overlap, and a Hanning window. The Hanning window was calculated using:

$$window(i+1) = 2.0*(0.5-0.5*\cos((2\pi/1024)*i)), \text{ where } i=0 \text{ to } 1023 \quad (2)$$

and applied to each ensemble prior to calculating the FFT amplitude. The resulting averaged amplitude of the FFT was converted to PSD (psi<sup>2</sup>/Hz) using:

$$PSD(i) = (amplitude(i)^2 * 1024 / sample\_rate) / 2, \text{ where } i=1 \text{ to } 511 \quad (3)$$

and frequency values defined as:

$$f(i) = (sample\_rate / 1024) * i, \text{ where } i=1 \text{ to } 511 \quad (4)$$

The sound pressure level (SPL) was calculated using:

$$SPL(i) = 20*\log_{10}(amplitude(i) / 2.90075e-9), \text{ where } i=1 \text{ to } 511 \quad (5)$$

For the 3D continuous distribution of PSP, the SPL calculation was performed at every vertex that had valid data and a special PLOT3D file was generated for each data point with SPL level at each vertex for every frequency in the bin. Sound pressure level was used to enhance data visualization. A special PSP viewer was developed to permit stepping through the frequencies and visualizing the SPL distribution in 3D. To enable conventional PSD plot comparisons of the conventional dynamic data and the PSP dynamic data, virtual dynamic pressure taps were generated 0.3" to the left (i.e. PSPLD10) and right (i.e. PSPRD10) of the transducers (i.e. D10) on the cavity floor and 0.3" above and below the transducers on the side wall. The virtual dynamic data were extracted from the 3D file and stored as PSD at each frequency in a text file for each location.

## IV. Experimental Results

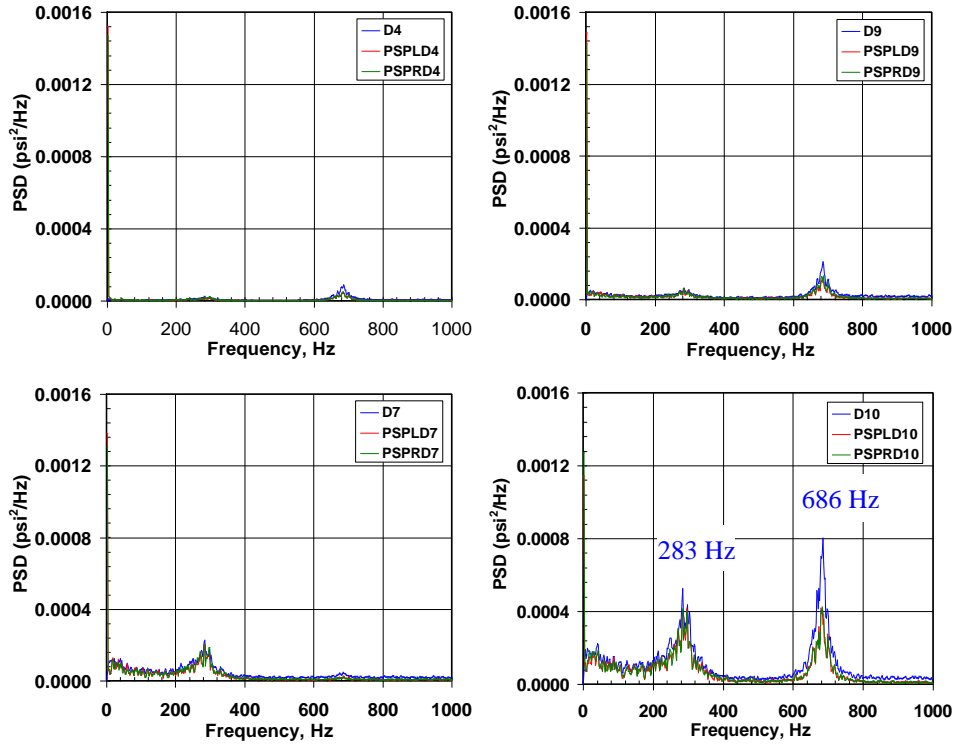
### A. Dynamic Pressure Measurement Comparisons

The validation of the dynamic PSP results will be made by comparing the virtual dynamic pressure data from the PSP (left and right of the transducer location) with nearby dynamic transducers. The following plots present data comparisons along the centerline of the cavity at four axial stations for two Mach numbers and with the flow-through inlets 100% open and blocked. The dynamic transducer peak frequencies are indicated in one of the four plots and are representative for all four locations. Figure 6 presents data at Mach 0.9 and 100% open for the three angles of attack and 0 deg sideslip. There are two dominant frequencies at all angles of attack with the magnitude increasing towards the downstream end of the cavity. Rossiter's calculation (Ref. 15) for a constant l/d cavity at Mach 0.9 predicts two dominate frequencies at 255 and 667 Hz. Even though the test article has a variable l/d over a portion of the cavity, the Rossiter tones nearly match the test data peaks. The PSP data aligns very well with the transducer data when examining the frequency distribution. However, the magnitude of the peaks from the PSP data are low at the highest frequency peak and match the lowest peak. Also note that the D7 location indicates only one dominate frequency and that being the lower one. More discussion on this will be presented in the next section. Figure 7 is typical for all conditions at Mach 1.3 with inlets 100% open. The data indicate a very quiet bay as compared to Mach 0.9, although with a small frequency peak at 917 Hz.

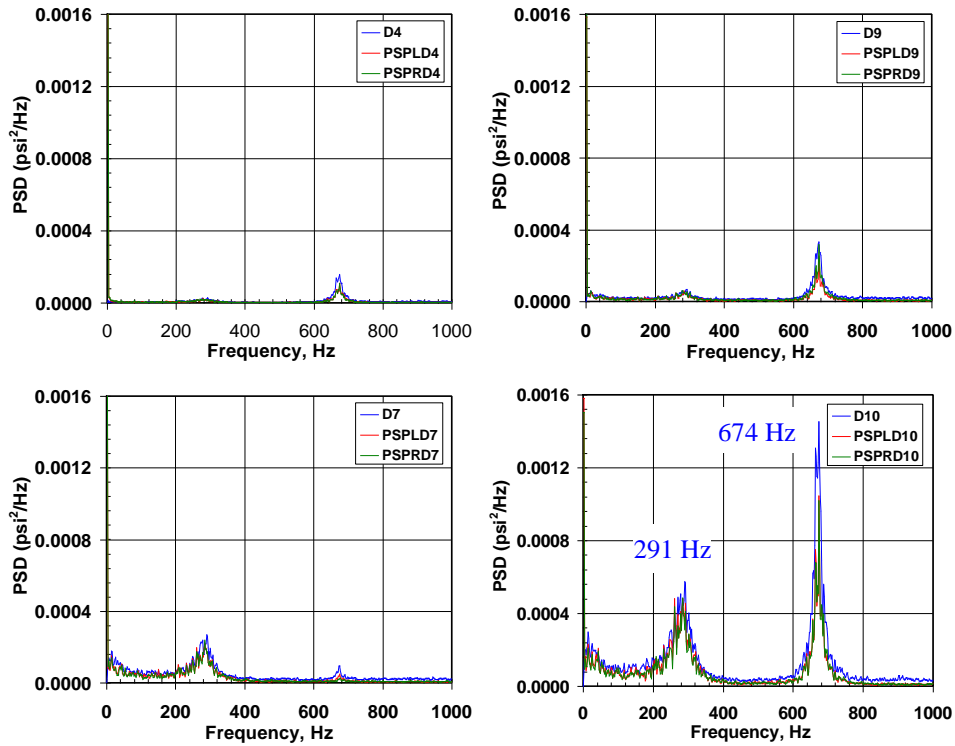
Comparisons at Mach 0.9 and 1.3, 100% blocked, are presented in Figs. 8 and 9, respectively. Both conditions indicate two dominate frequencies and are believed to be result of "bottle top" whistling from the inlets with a low primary frequency and a higher harmonic. One case that does not follow this example is Mach 0.9 at 0 deg angle of attack. The "whistle" tone magnitude is significantly lower and the second frequency (not a harmonic) is likely a bay cavity effect resulting from inlet spillage. Although not presented, the second frequency peak is gone at 5 deg angle of attack. At Mach 1.3 the dominate whistle tone is at the higher frequency for - 2 deg angle of attack and reverses at 0 deg angle of attack. The effect of sideslip on cavity flow is presented in Fig. 9c. The strong tones in Fig. 9a drop considerably in magnitude and an interesting double tone occurs at the second harmonic.

With this being the first dynamic PSP test in 16T and the data download speed from the cameras not optimized, the length of image recording was limited to 2000 or 3000 frames/sec for 4.1 and 1.37 second duration, respectively. However, one data point was acquired at Mach 1.3 (for open and blocked) at 4000 frames/sec for 4.1 seconds (15GB data file per camera) to permit evaluation of a longer data record. A comparison of Kulite® and PSP data for the two sample rates and record lengths is presented in Fig.10. The vertical axis was magnified to illustrate the noise reduction in the PSP data as a result of more FFT averaging for the longer sample time. Although not presented, the peak frequencies and magnitudes matched between sample rates.

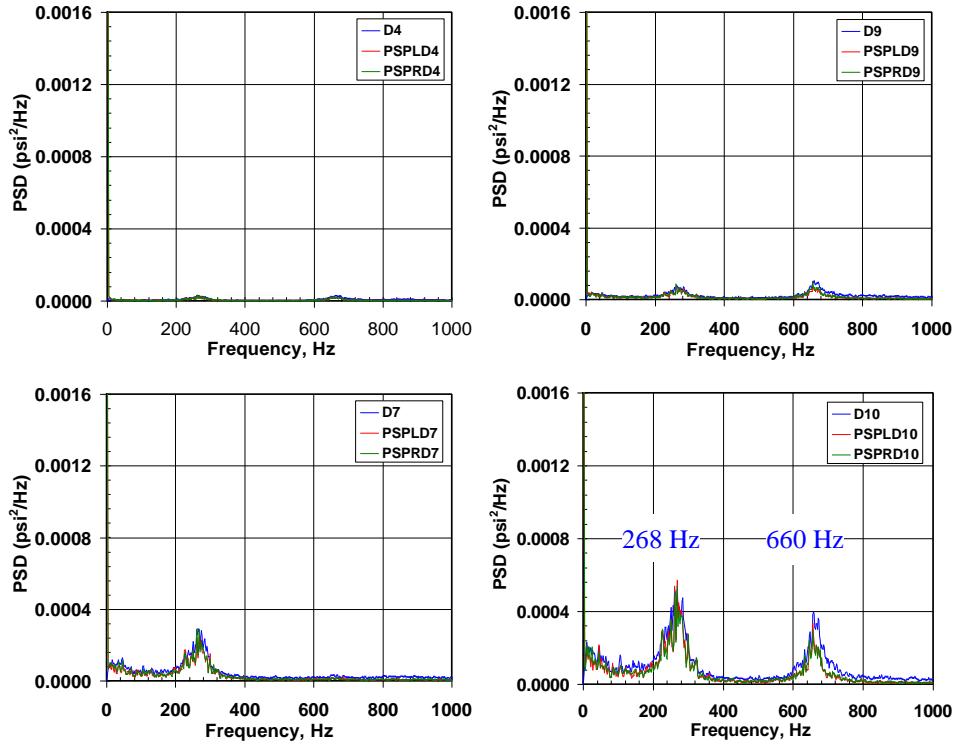
Since the PSP is an absolute pressure sensor, data were acquired at two Reynolds numbers for Mach 0.9 to evaluate the impact on dynamic PSP measurements. A comparison of data at Reynolds number 2 and 2.5 million per foot is presented in Fig. 11 for 100% open and blocked configurations. For the 100% open case, the dynamic transducer indicates a difference in magnitude at the lower peak frequency while the PSP data agree very well for both peak frequencies. Researchers have reported little effect of Reynolds number on acoustic spectra generated by rectangular cavities in subsonic flow (Ref. 16). For the 100% blocked case, the dynamic transducer and PSP data indicate a change in the frequency location for the second peak with Reynolds number and agree very well with each other.



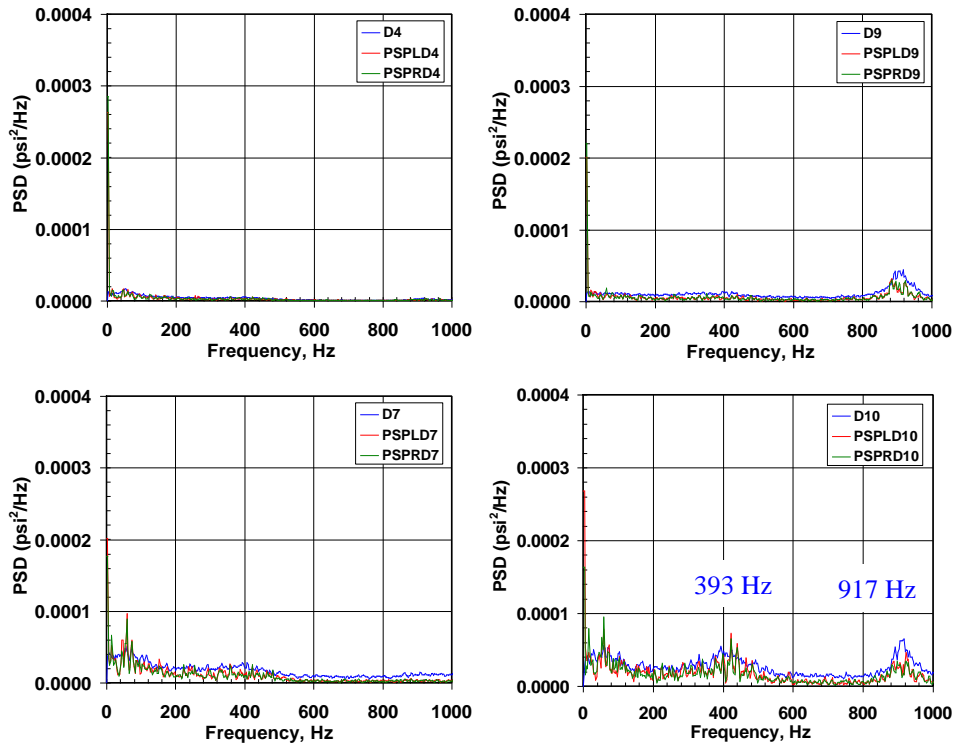
a. Alpha -2 deg, Beta 0 deg.  
 Figure 6. PSD Comparison, Mach 0.9, 100% Open.



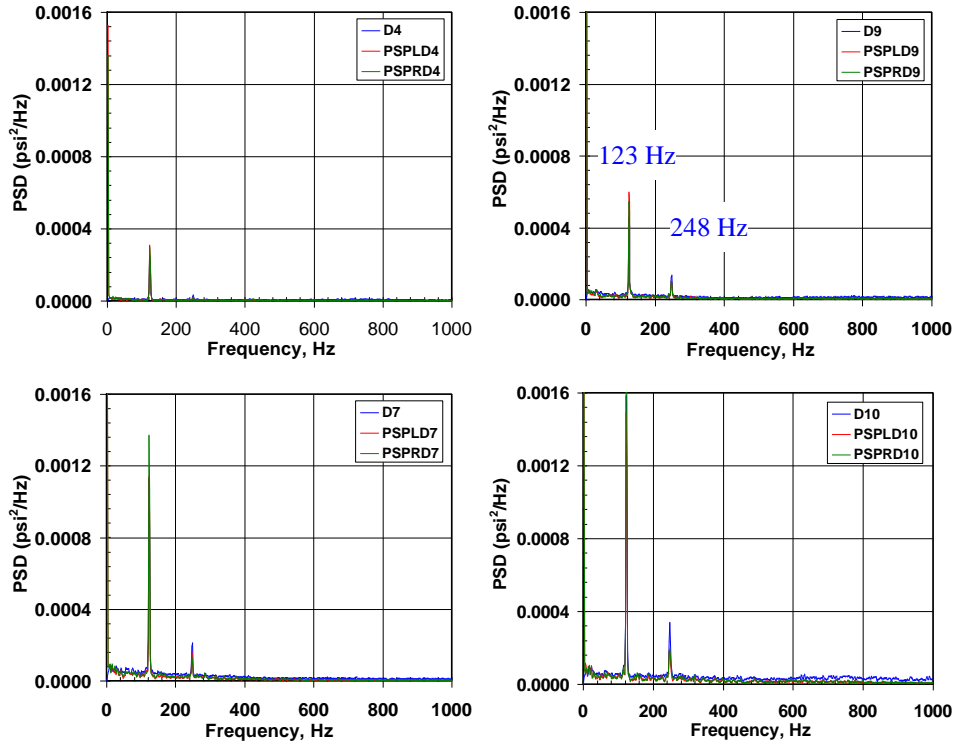
b. Alpha 0 deg, Beta 0 deg.  
 Figure 6. Continued.



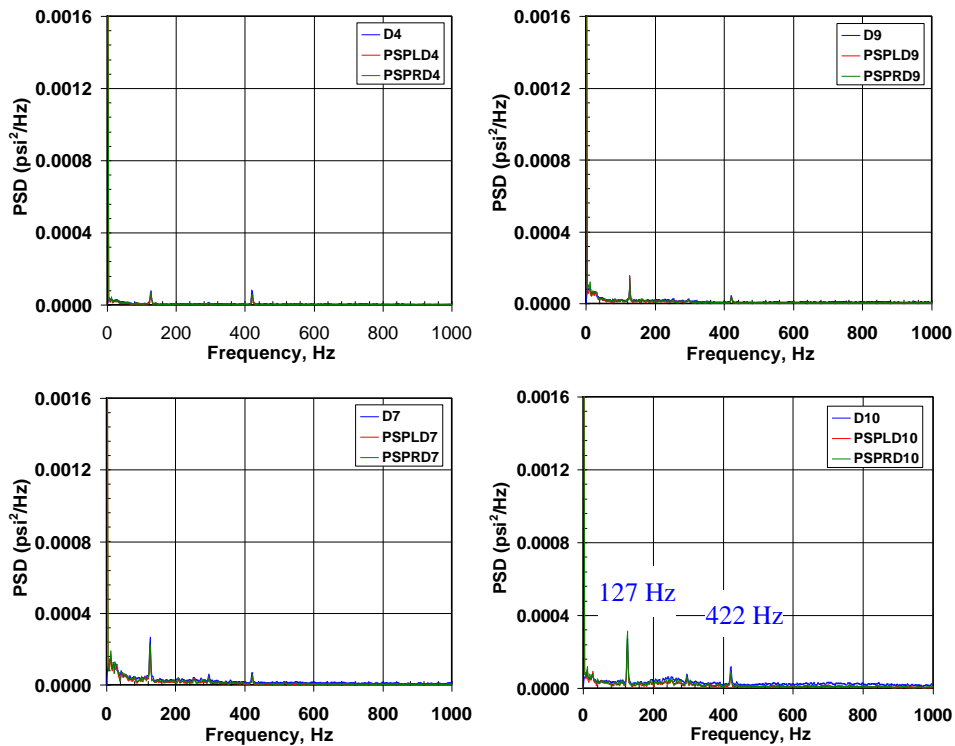
c. Alpha 5 deg, Beta 0 deg.  
Figure 6. Concluded.



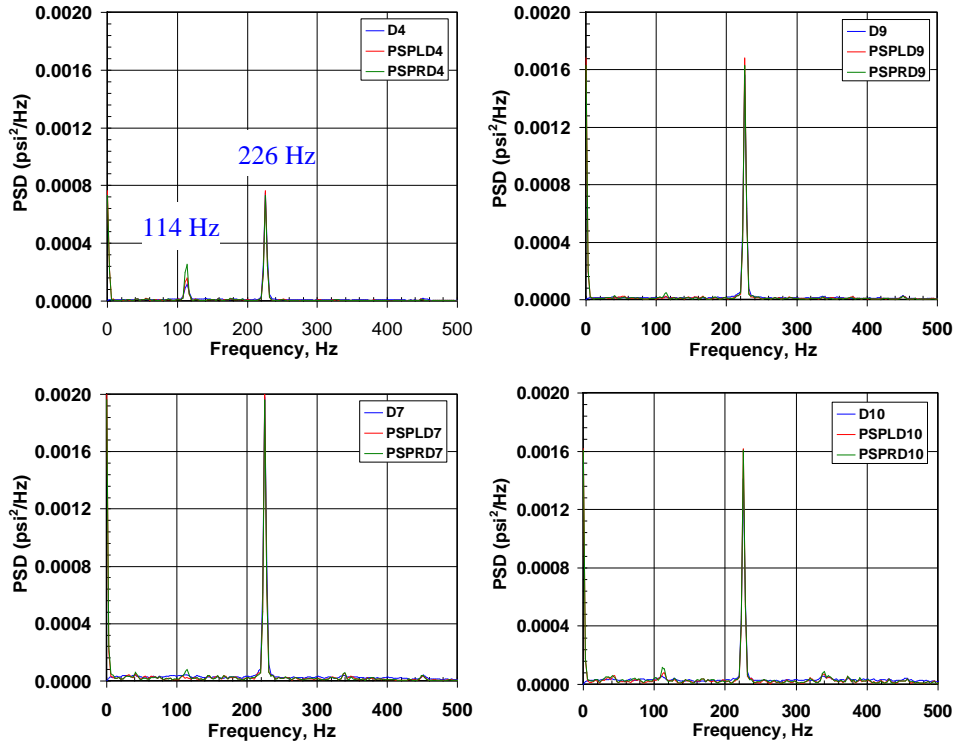
a. Alpha 5 deg, Beta 0 deg.  
Figure 7. PSD Comparison, Mach 1.3, 100% Open.



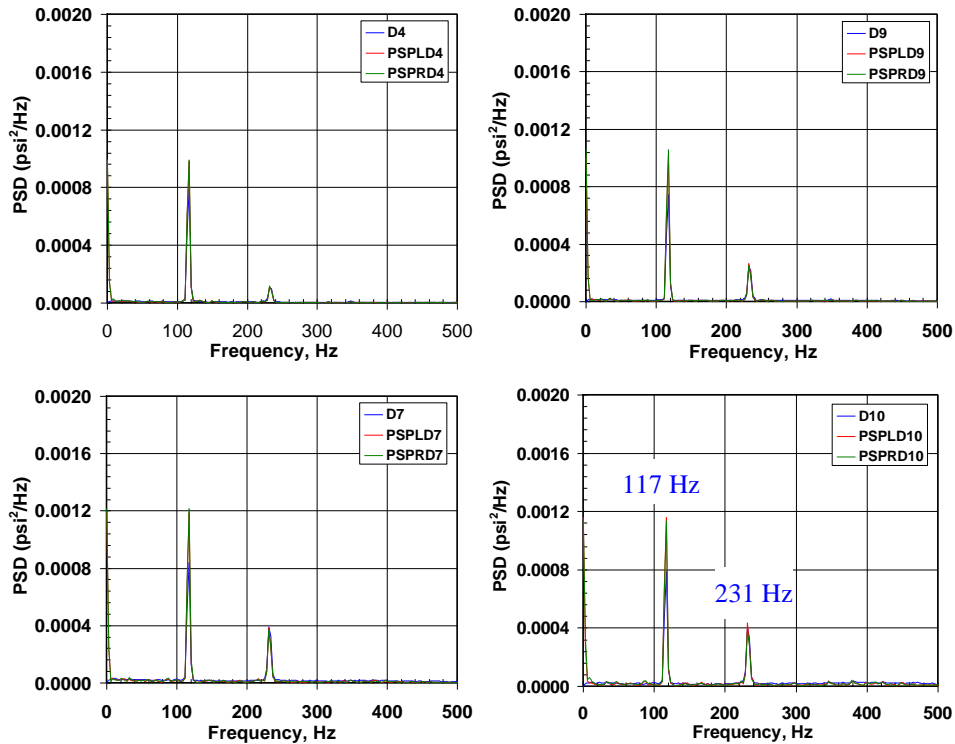
a. Alpha -2 deg, Beta 0 deg.  
 Figure 8. PSD Comparison, Mach 0.9, 100% Blocked.



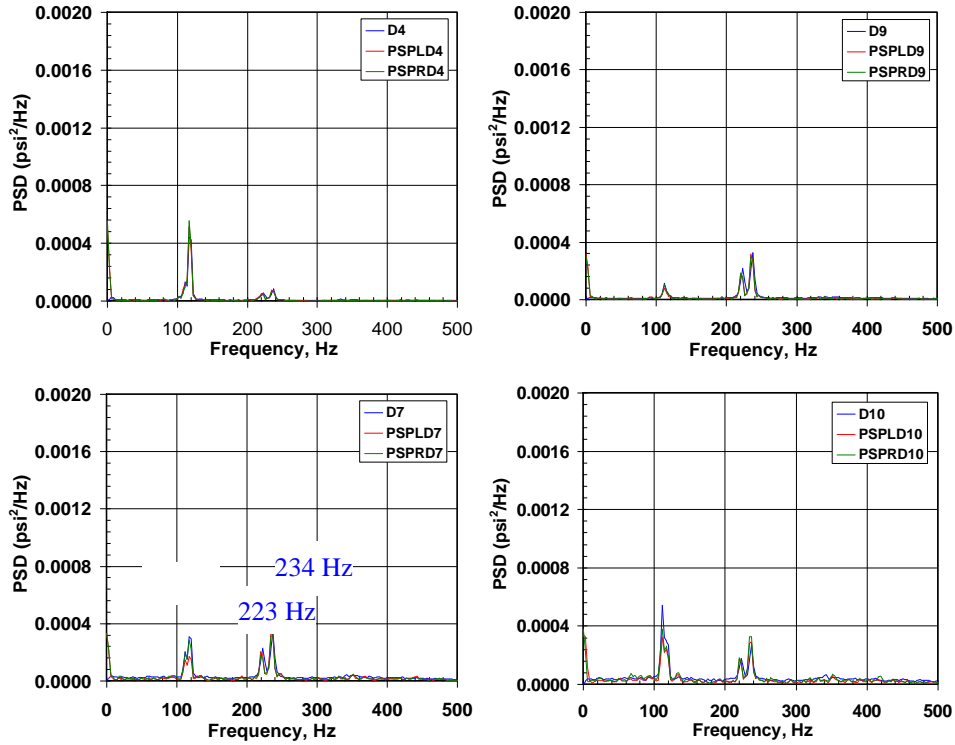
b. Alpha 0 deg, Beta 0 deg.  
 Figure 8. Concluded.



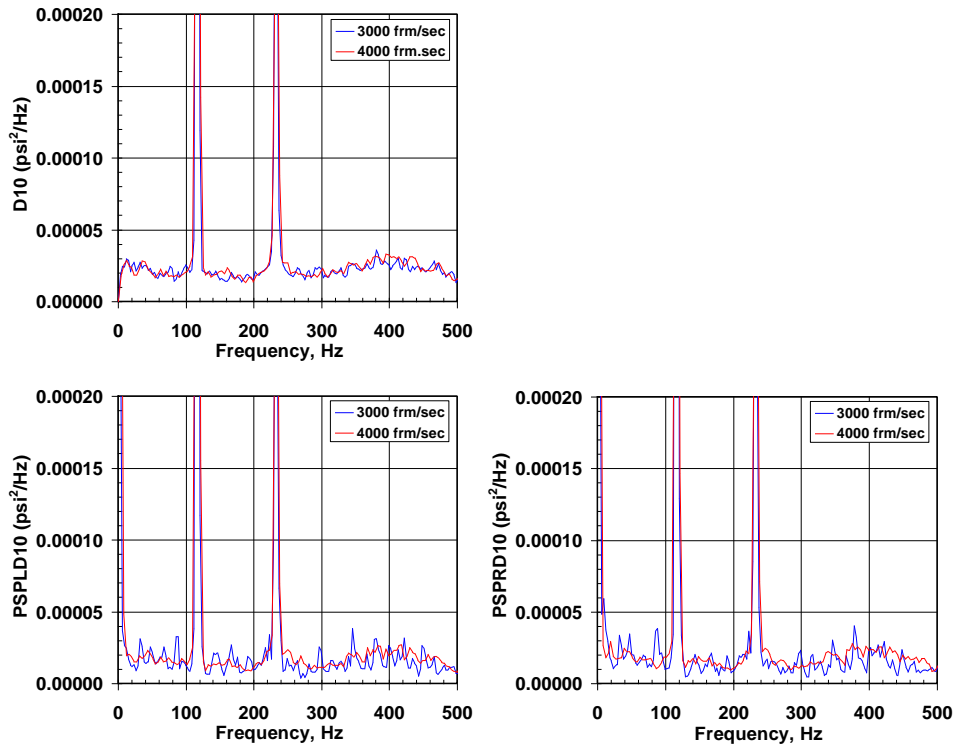
a. Alpha -2 deg, Beta 0 deg.  
 Figure 9. PSD Comparison, Mach 1.3, 100% Blocked.



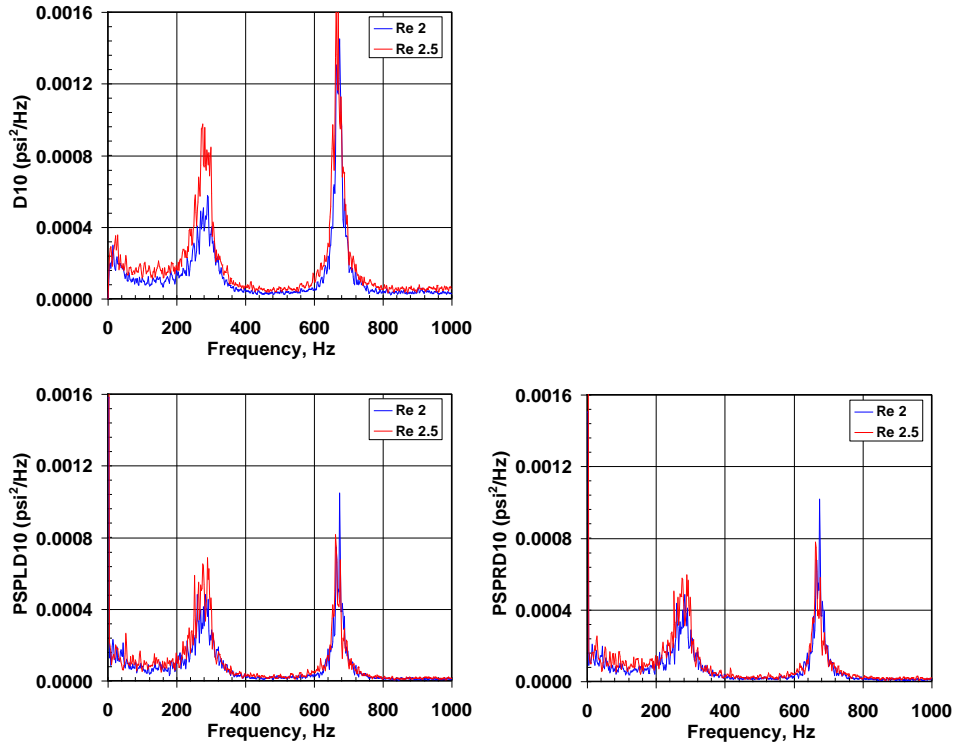
b. Alpha 0 deg, Beta 0 deg.  
 Figure 9. Continued.



c. Alpha -2 deg, Beta 2 deg.  
Figure 9. Concluded.

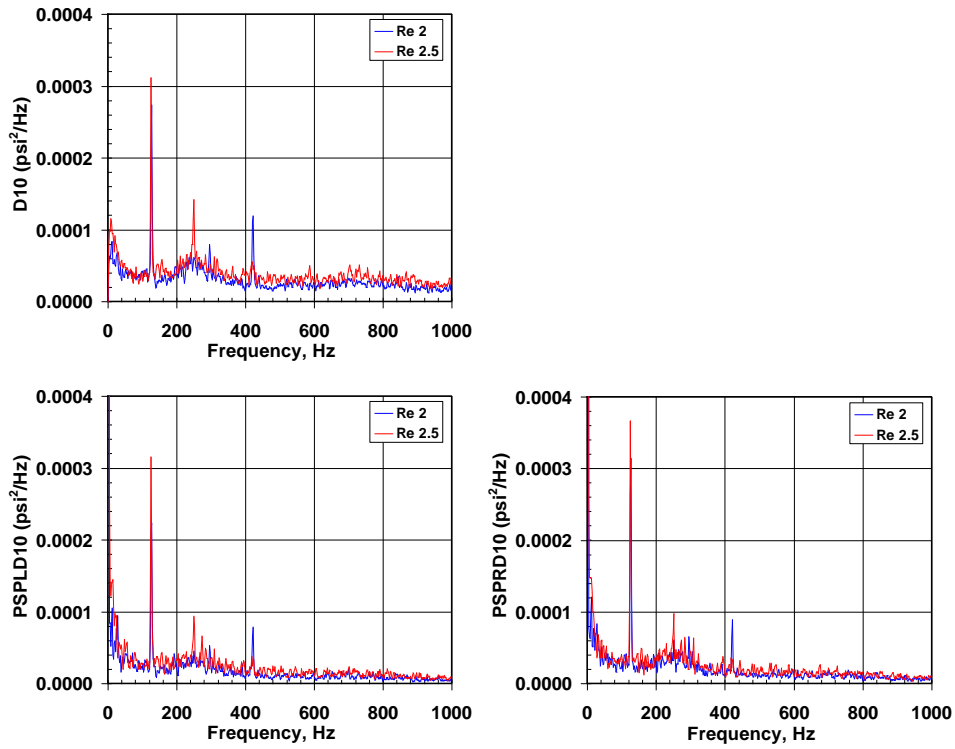


a. Mach 1.3, Alpha 0 deg, Beta 0 deg.  
Figure 10. Sample Rate and Length Comparison.



a. 100% Open.

Figure 11. Reynolds Number Effect, Mach 0.9, Alpha 0 deg, Beta 0 deg.



b. 100% Blocked.

Figure 11. Concluded.

## B. Full Surface Sound Pressure Level Distributions

One of the advantages of PSP over point source measurements is the ability to acquire high spatial resolution data over the test article surface. Typical launch vehicle dynamic pressure tests have a limited number of transducers (located in axial rows at several azimuth angles). The fluctuating pressures are integrated at each station over lengths that are difficult to determine and result in conservative fluctuating load distributions. Aircraft configurations, such as this article, are more limited by space and surface thickness when instrumenting with dynamic transducers. In addition, data can only be acquired at instrumented locations. Presenting the vast information available from dynamic PSP in a document is difficult. However, a sample of the results at conditions discussed in the previous section is presented to demonstrate a new way to visualize dynamic pressure data.

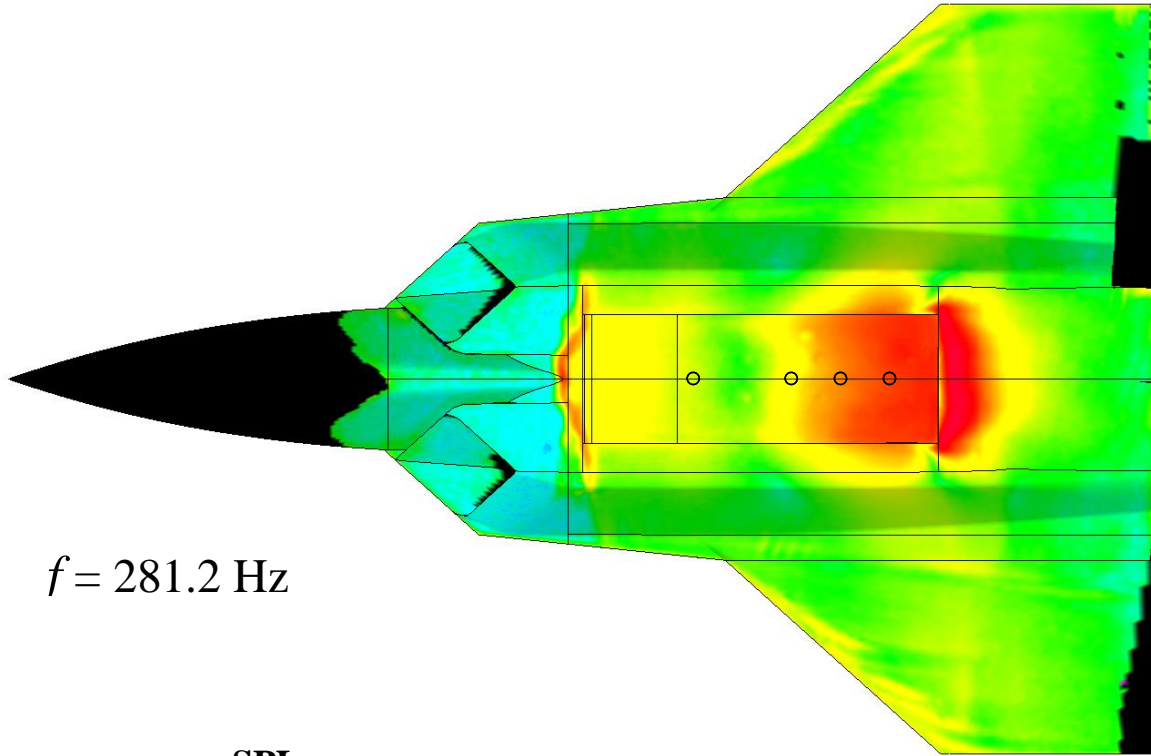
The SPL distribution at the two peak frequencies from the dynamic PSP data are presented in Fig. 12 for Mach 0.9 and 100% open configuration for angles of attack -2, 0 and 5 deg. The small circles in the weapons bay indicate the location of the dynamic pressure transducers discussed in the previous section. Recall in Fig. 6 that the third axial location (D7) indicated only one strong peak and that being the lower frequency. Examining the distribution in Fig. 12, the D7 location is in a region of wave cancellation at the higher frequency. Interestingly, the effect extends out of the cavity onto the lower fuselage surface. A second region of cancellation can be seen on the forward ramp. The detail of dynamic pressure fluctuation is excellent and provides significantly more insight into the cavity (and fuselage) flow. A person would have difficulty examining the equivalent of 250,000 PSD plots to visualize what is presented from PSP. The distribution at Mach 1.3 is presented in Fig. 13 for 5 deg angle of attack. Notice the significant reduction in SPL and the wave cancellation that exists at the higher frequency.

The SPL distributions with the 100% blocked configuration are presented in Figs. 14 and 15 for Mach 0.9 and 1.3, respectively. The dynamic energy is significantly more affected by the blocked inlet than the bay acoustics. The highest SPL levels occur around the inlet and propagate downstream on the fuselage. Also, significant vortical flow is present on the fuselage and along the wing leading edge. At Mach 1.3 there are several wave patterns that develop on the side of the fuselage with some interesting shapes. It would be impossible to capture these patterns with conventional transducers.

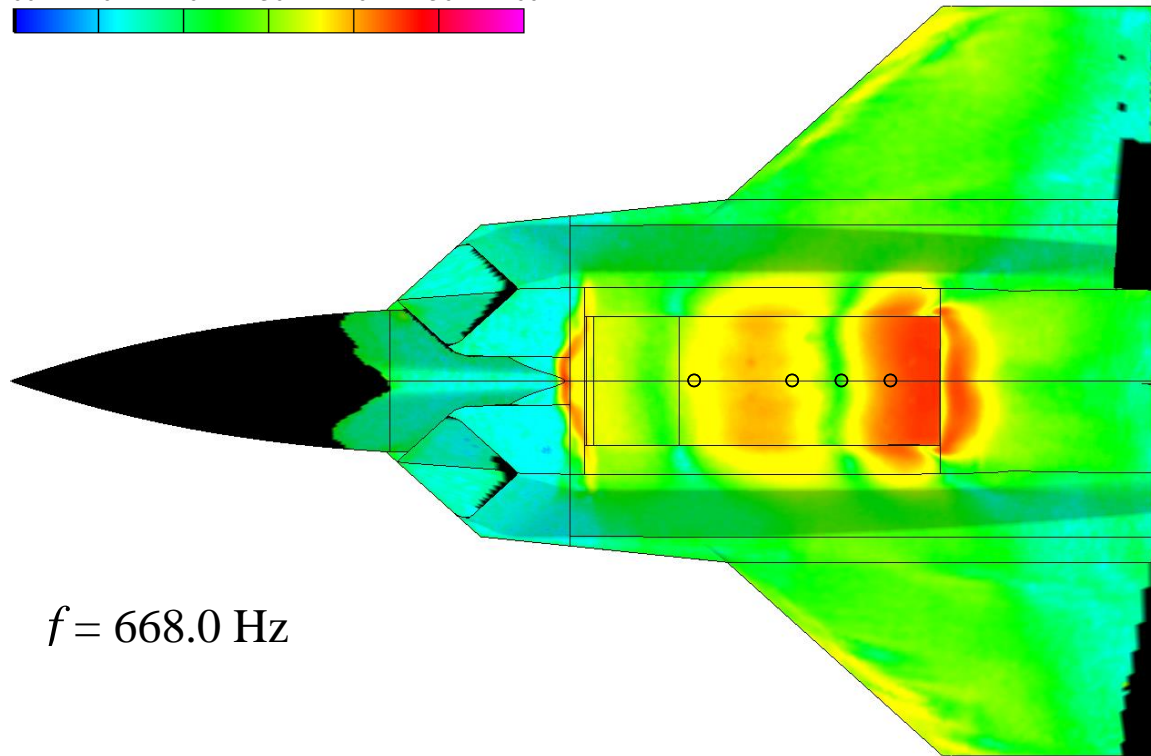
Another interesting feature was discovered for the 100% blocked configuration when the model was at 2 deg sideslip. Presented in Fig. 16 are SPL distributions for Mach 0.9 at several frequencies surrounding the first and second peaks. At the first peak frequency, the SPL increases around the right inlet (windward side) but the opposite occurs at the second peak frequency. While this is not a real world case, it demonstrates that the leeward inlet is beating more than twice as fast as the windward inlet. At Mach 1.3, a double tone was observed in the PSD plots (see Fig. 9c) for -2 deg angle of attack and 2 deg sideslip. For this condition, the frequencies around the first and second peaks are presented in Fig. 17. At the first peak frequency, the SPL starts to increase on the leeward inlet but switches to the windward inlet before degrading. At the second peak frequency, the leeward inlet has a peak and then shifts to the windward inlet at the little higher frequency, hence the double tone peak. For this test condition the second frequency appears to be a harmonic.

## C. Analysis Using Proper Orthogonal Decomposition

The power spectral density and sound pressure level at a set of points on the model yield important insight into the frequency content of a given time series. This technique, however, provides a somewhat limited understanding of the spatio-temporal nature of the dynamics of the entire system. In unsteady, turbulent flows, proper orthogonal decomposition (POD) provides for the extraction of relevant flow structures that present a characteristic temporal life cycle, as well as the frequency content of those flow features (Ref. 15). POD analysis has also lent itself to use as a filter of spurious data and noise in particle image velocimetry (Refs. 17 and 18), and has been extended to the dynamic PSP data for evaluation of benefit.

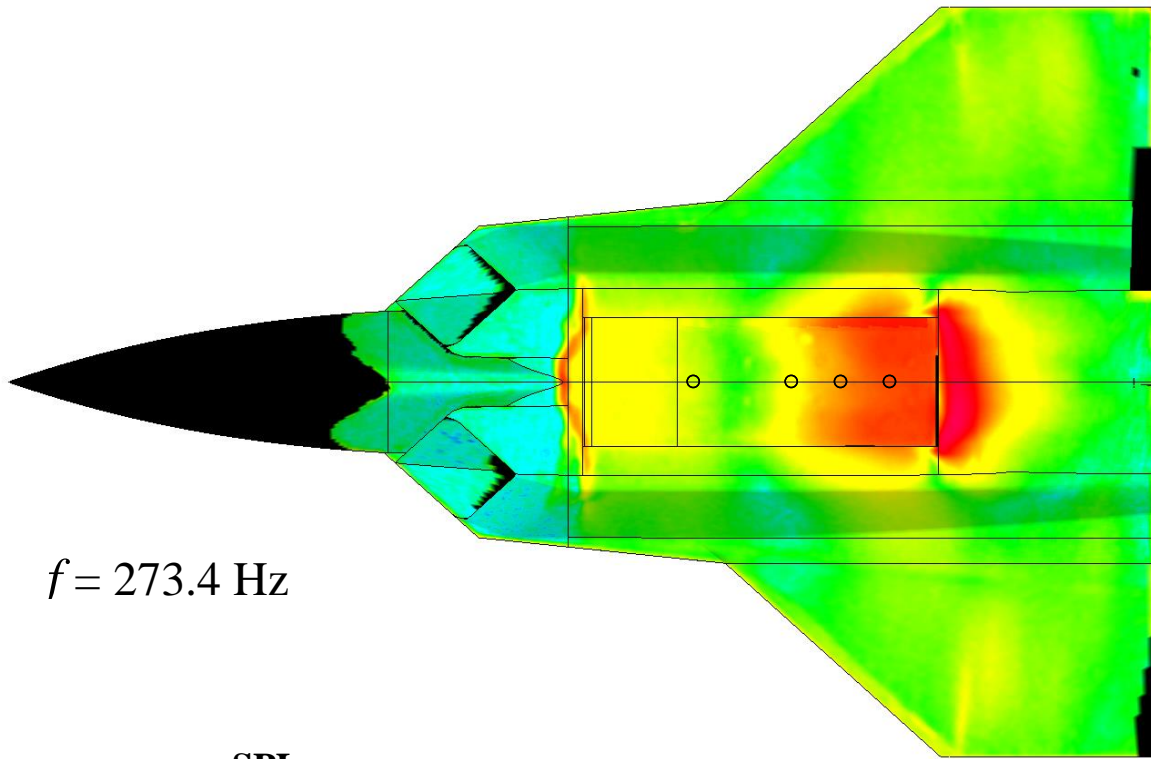


$f = 281.2$  Hz

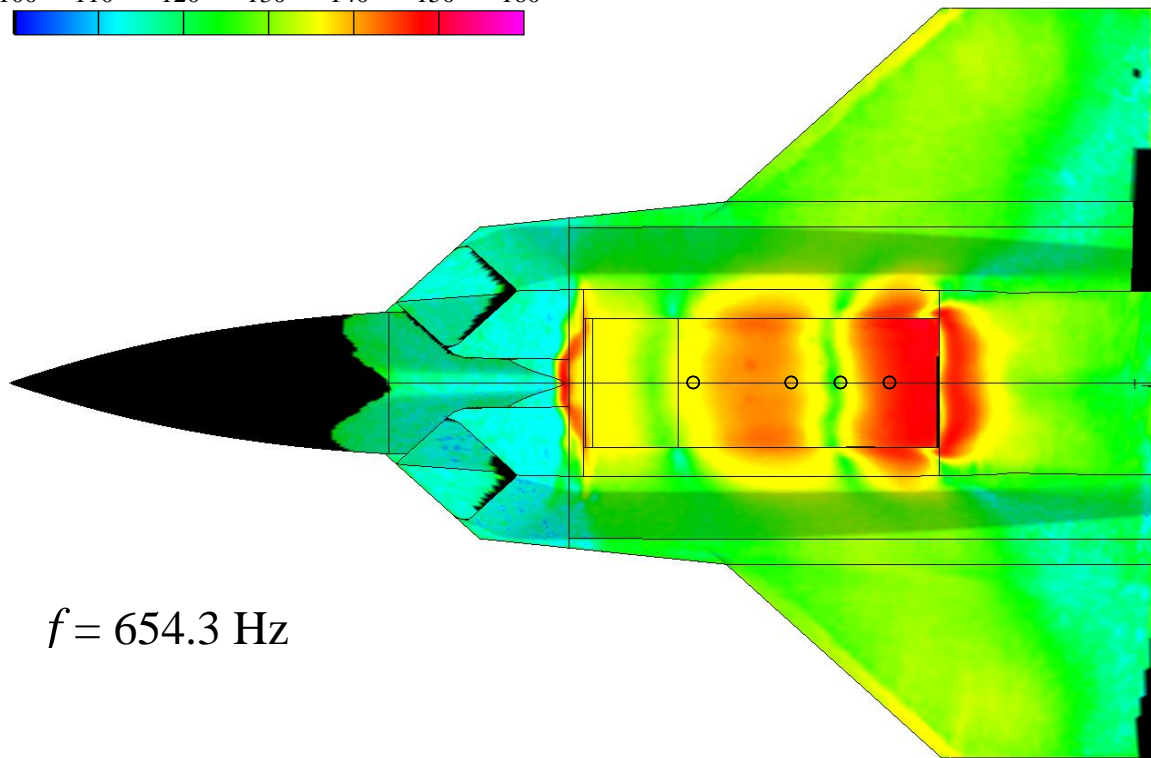


$f = 668.0$  Hz

a. Alpha -2 deg, Beta 0 deg.  
Figure 12. SPL Distribution, Mach 0.9, 100% Open.

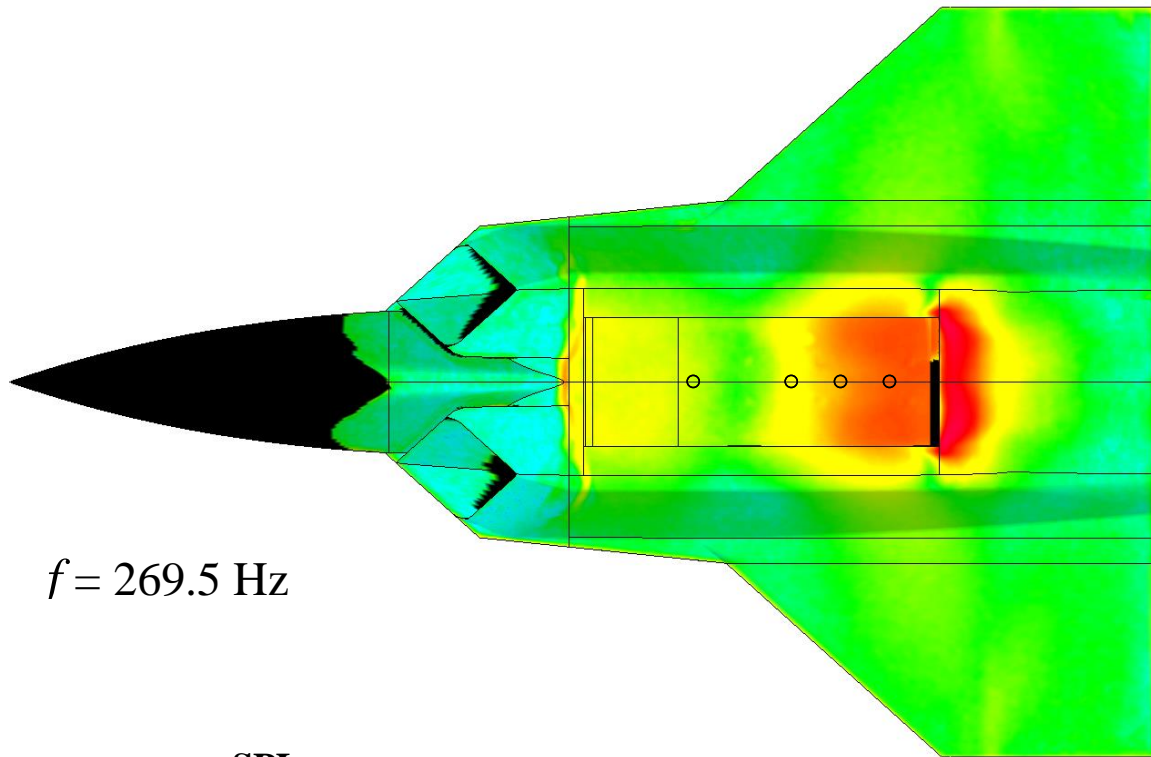


$f = 273.4$  Hz

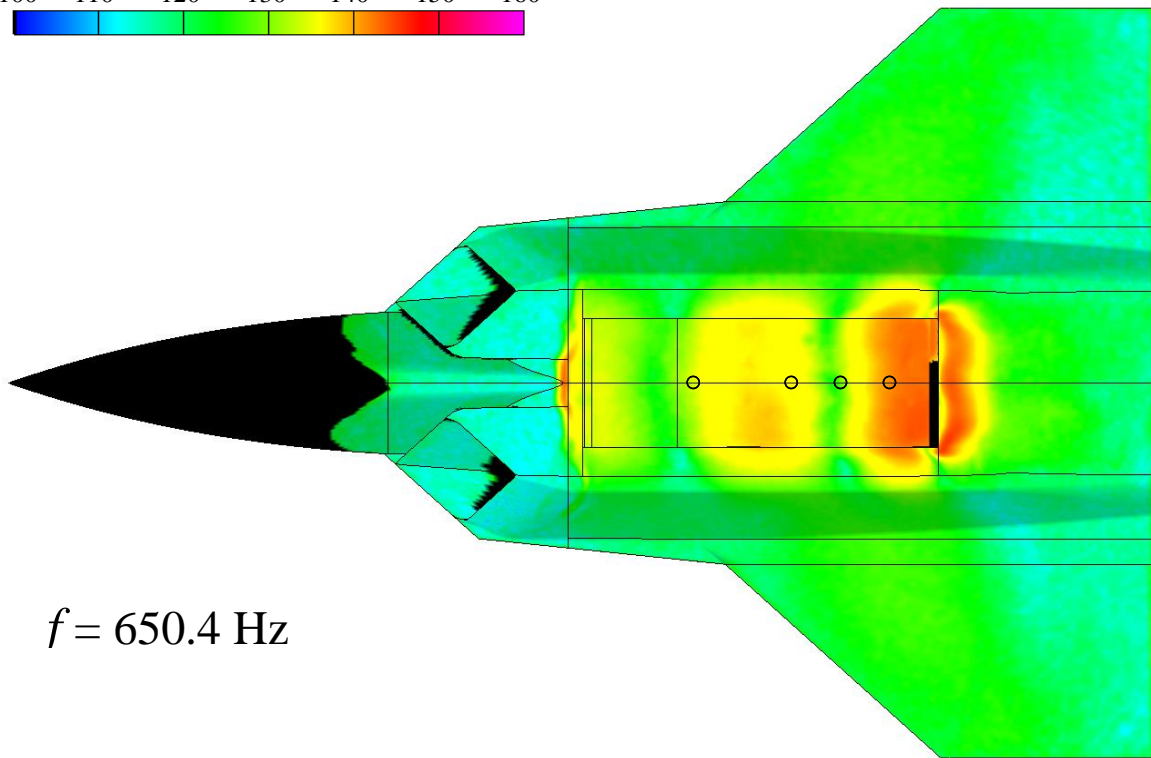


$f = 654.3$  Hz

**b. Alpha 0 deg, Beta 0 deg.  
Figure 12. Continued.**

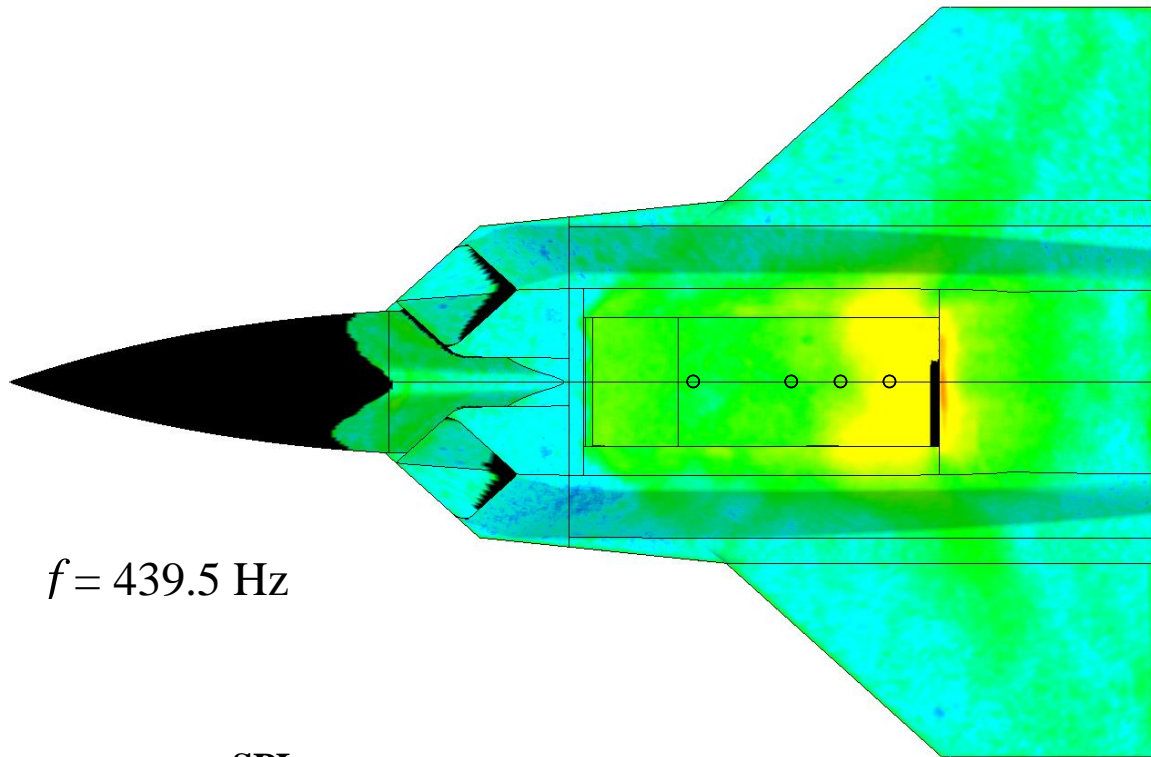


$f = 269.5$  Hz

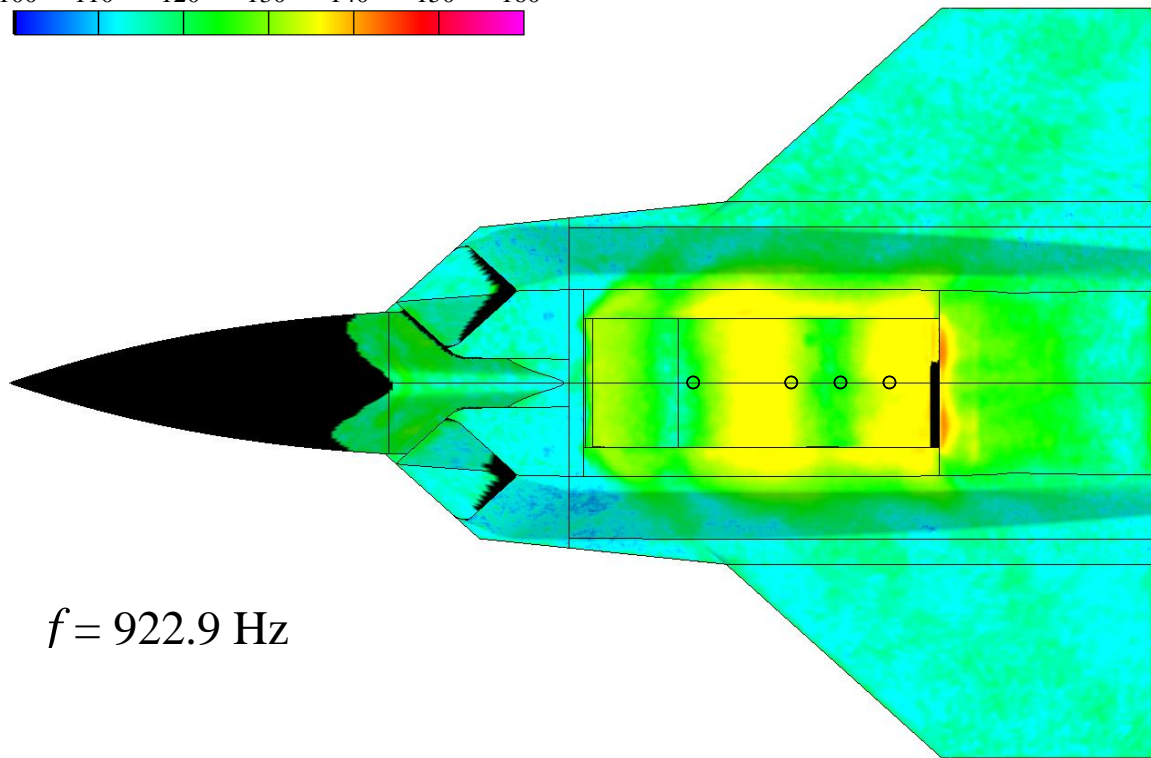


$f = 650.4$  Hz

c. Alpha 5 deg, Beta 0 deg.  
Figure 12. Concluded.

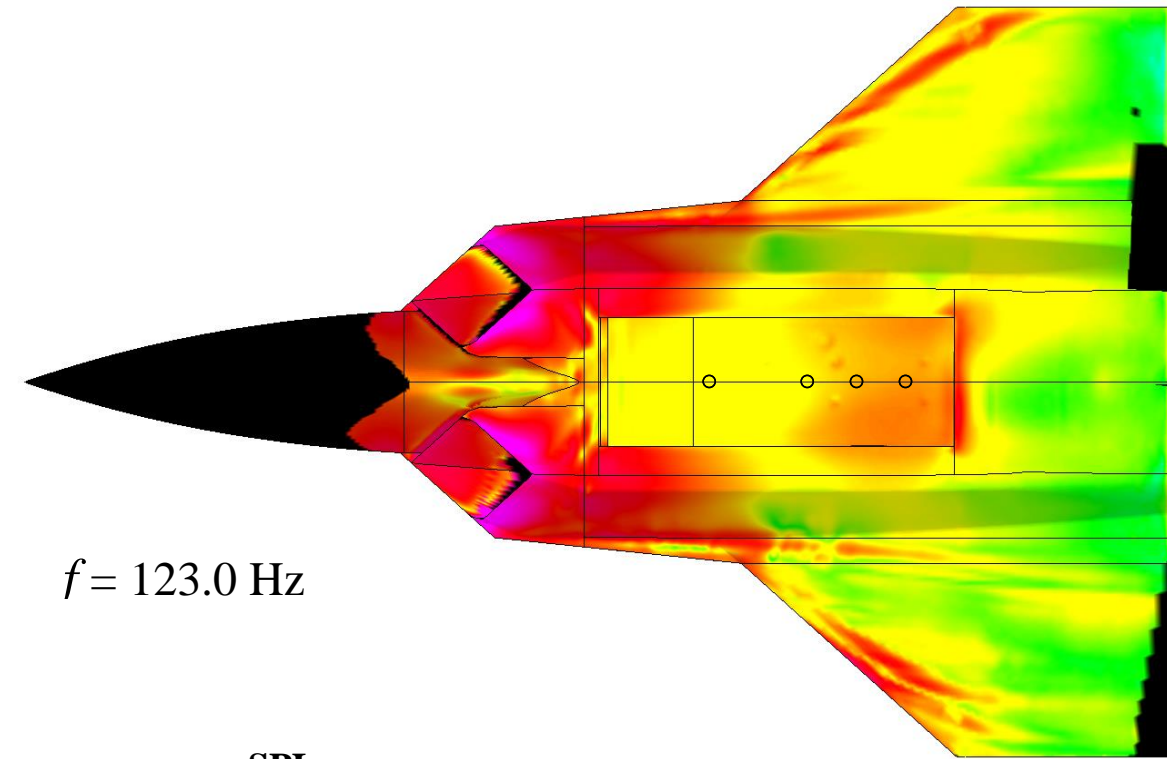


$f = 439.5$  Hz

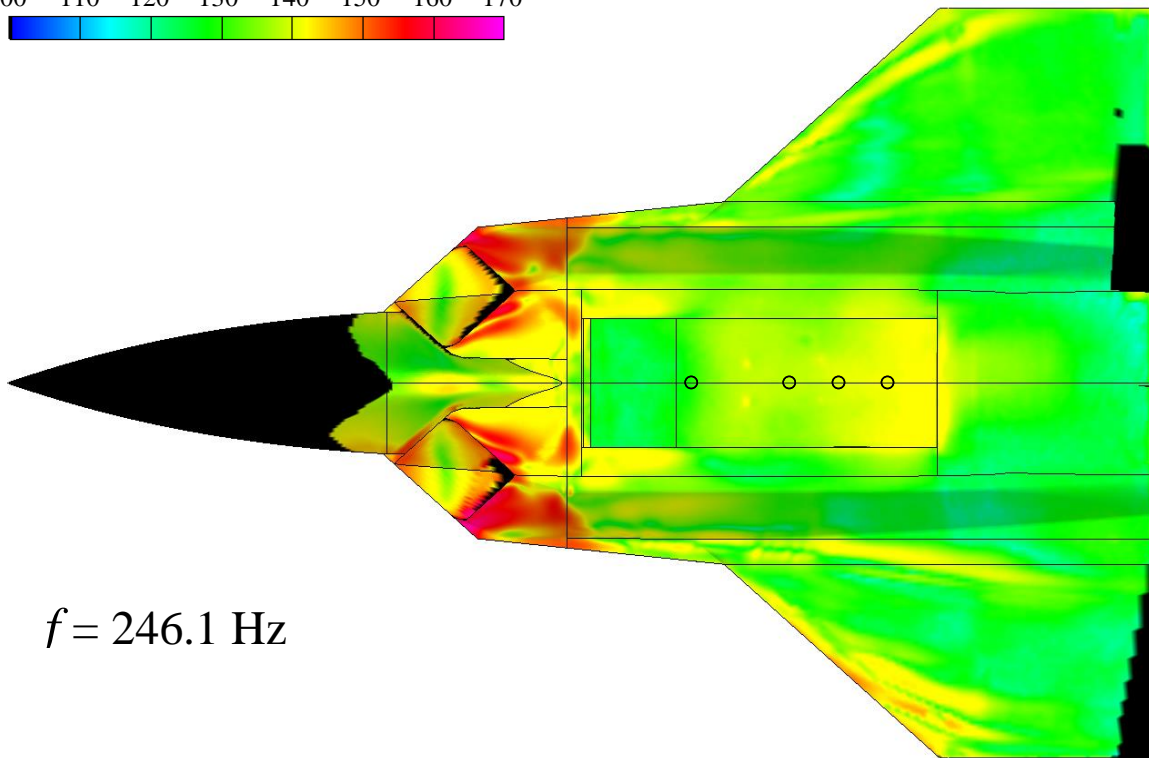
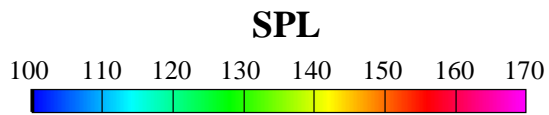


$f = 922.9$  Hz

a. Alpha 5 deg, Beta 0 deg.  
Figure 13. SPL Distribution, Mach 1.3, 100% Open.

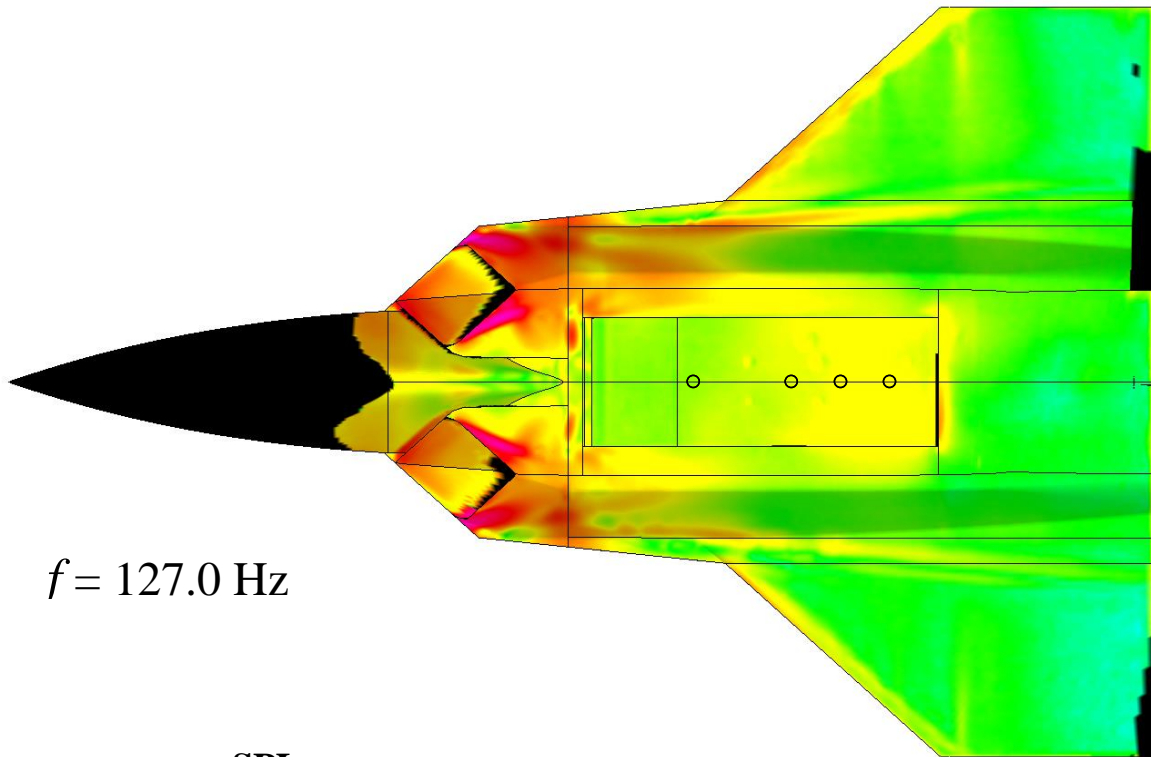


$f = 123.0$  Hz

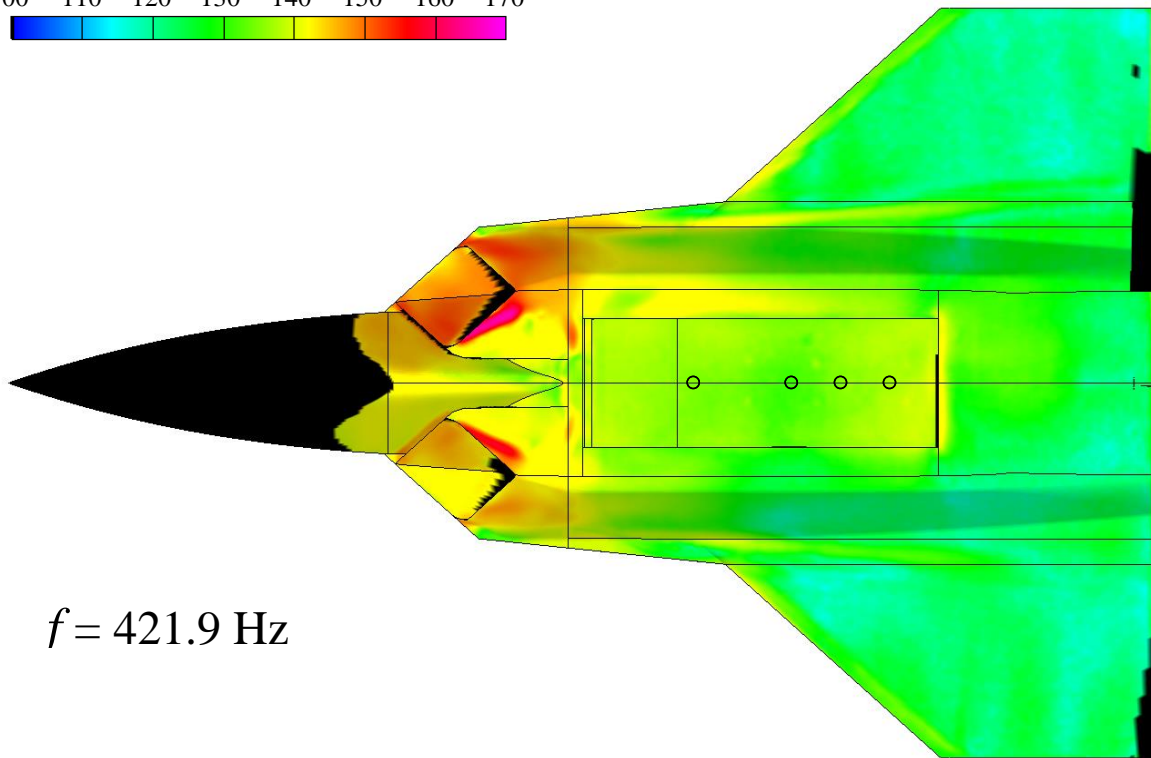
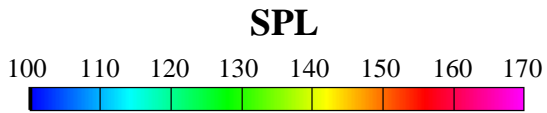


$f = 246.1$  Hz

a. Alpha -2 deg, Beta 0 deg.  
**Figure 14. SPL Distribution, Mach 0.9, 100% Blocked.**

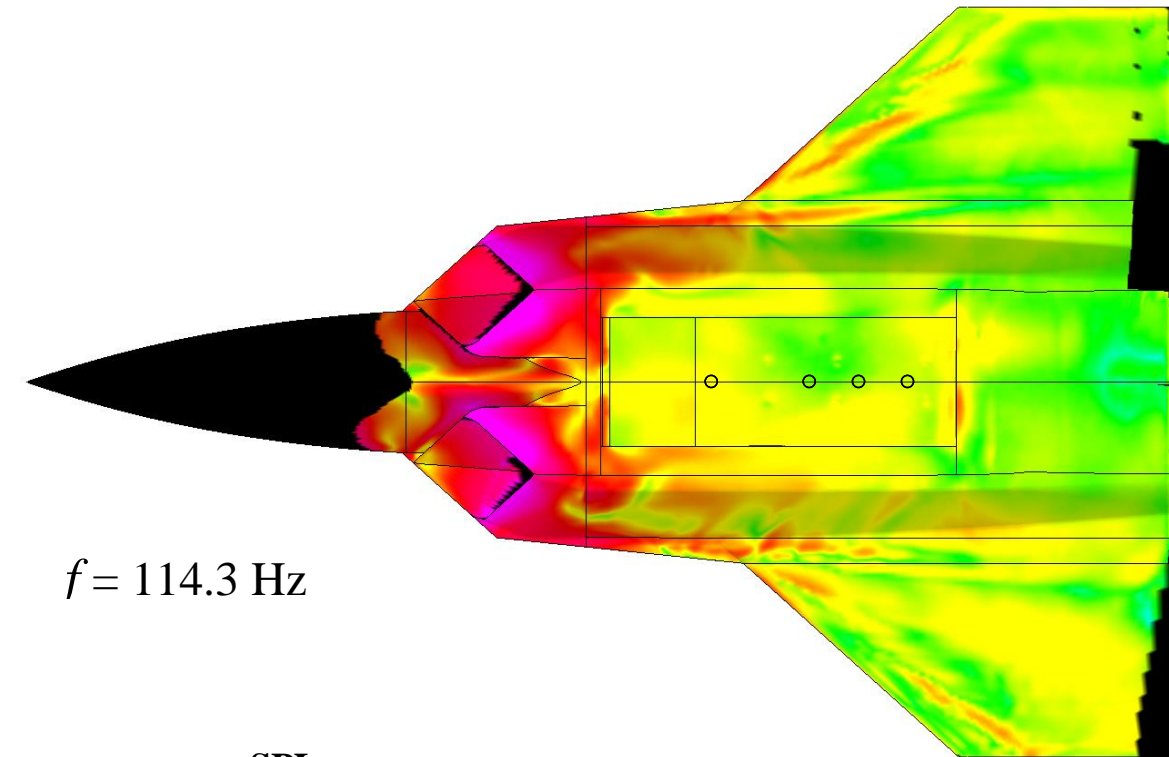


$f = 127.0 \text{ Hz}$



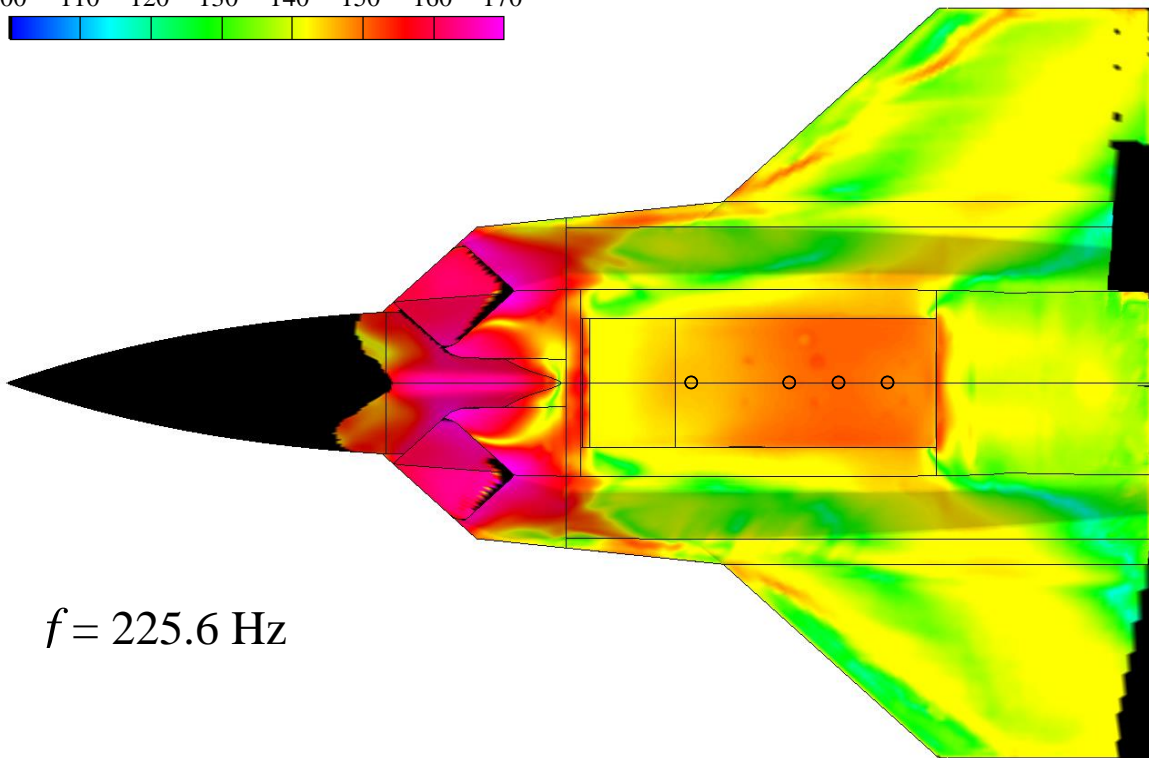
$f = 421.9 \text{ Hz}$

**b. Alpha 0 deg, Beta 0 deg.  
Figure 14. Concluded.**



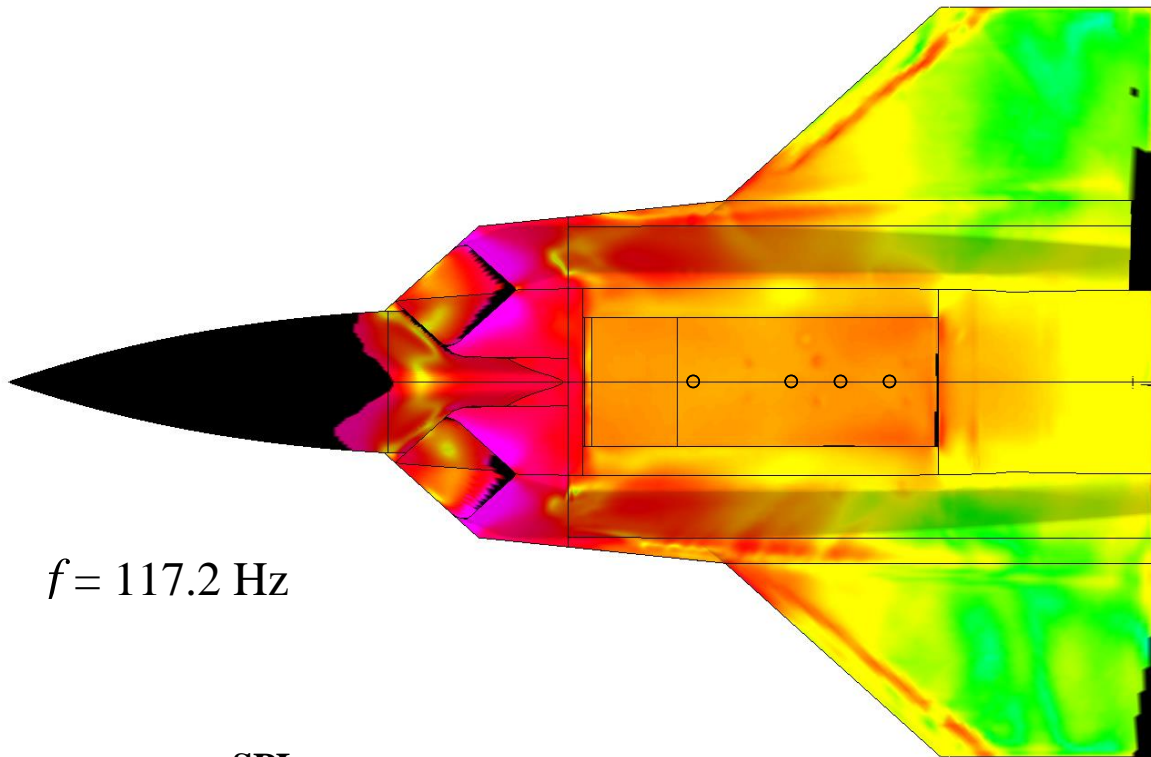
$f = 114.3$  Hz

**SPL**

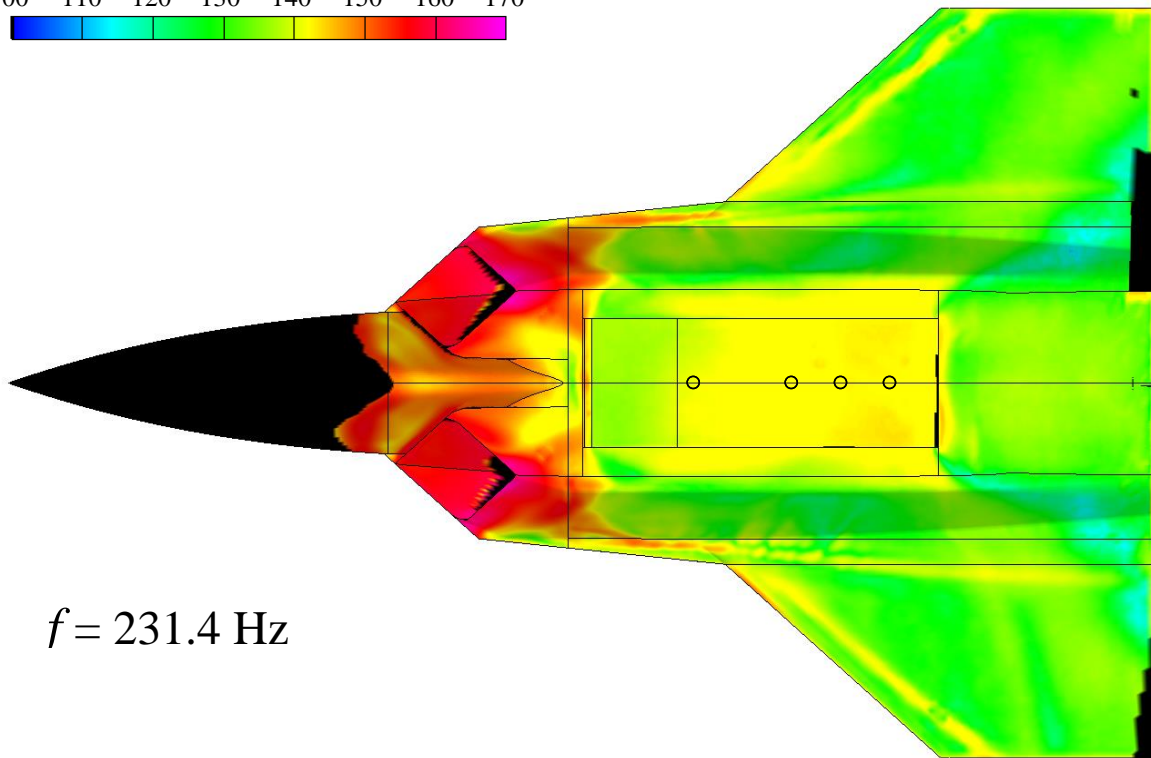
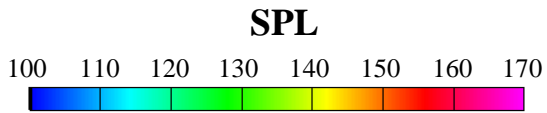


$f = 225.6$  Hz

**a. Alpha -2 deg, Beta 0 deg.**  
**Figure 15. SPL Distribution, Mach 1.3, 100% Blocked.**

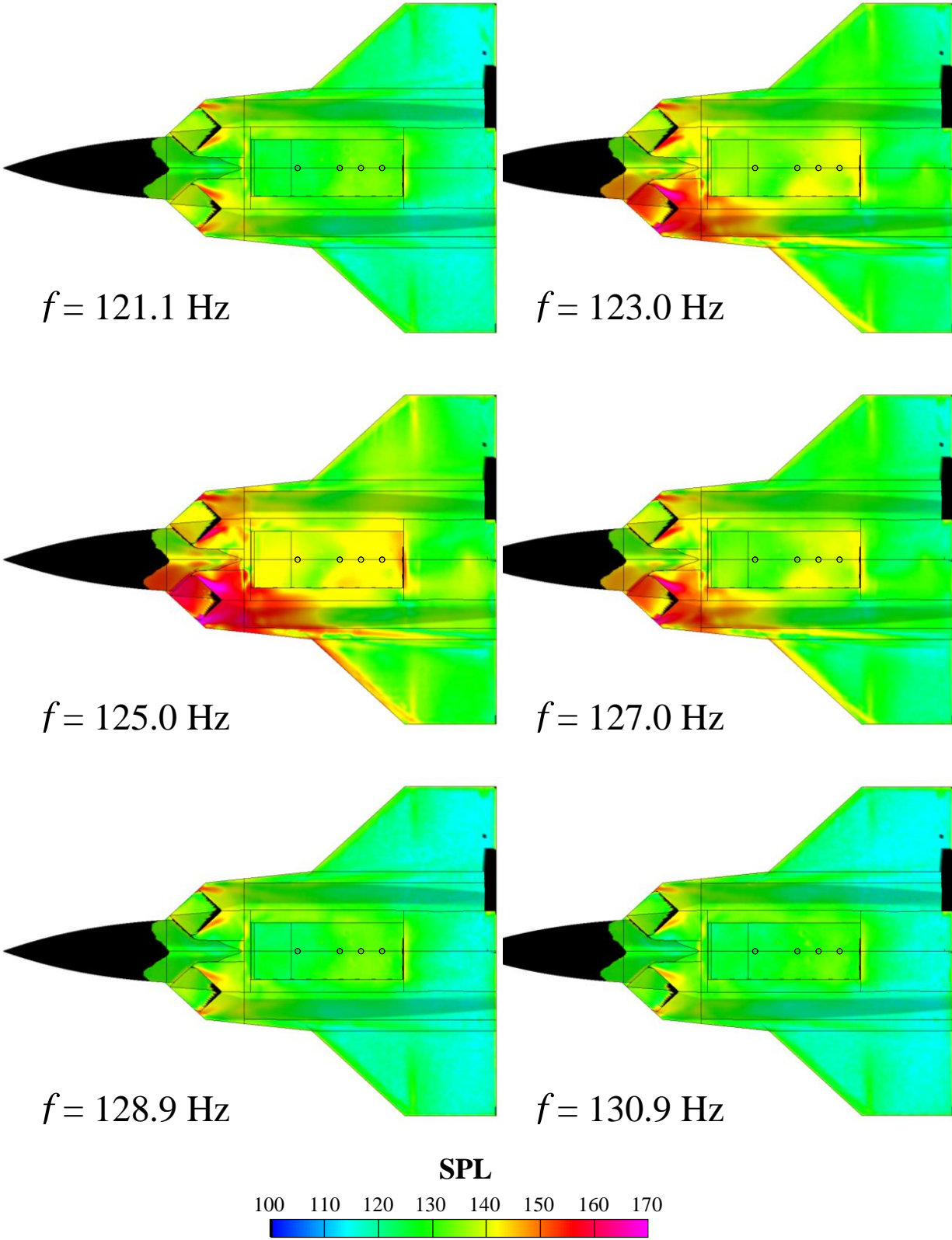


$f = 117.2 \text{ Hz}$

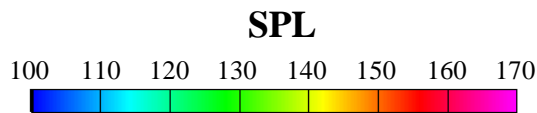
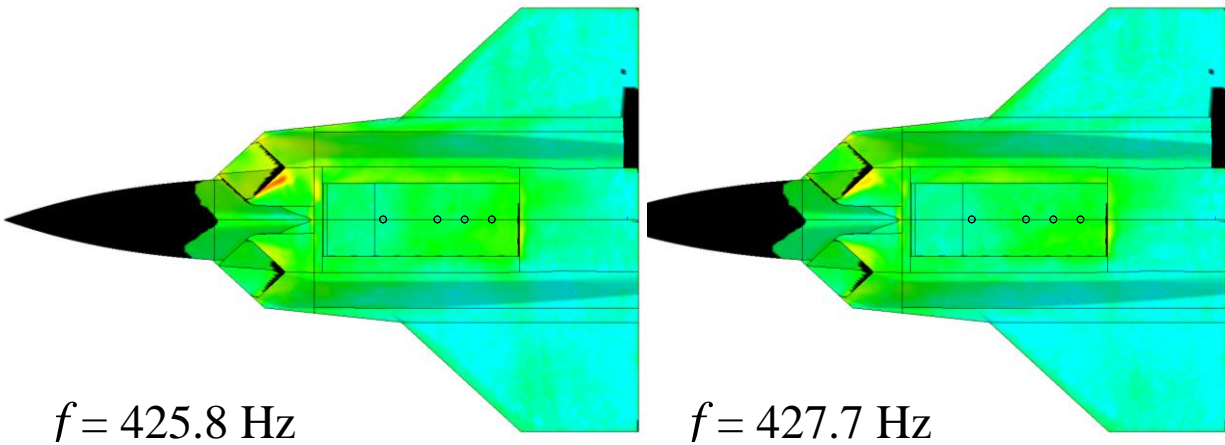
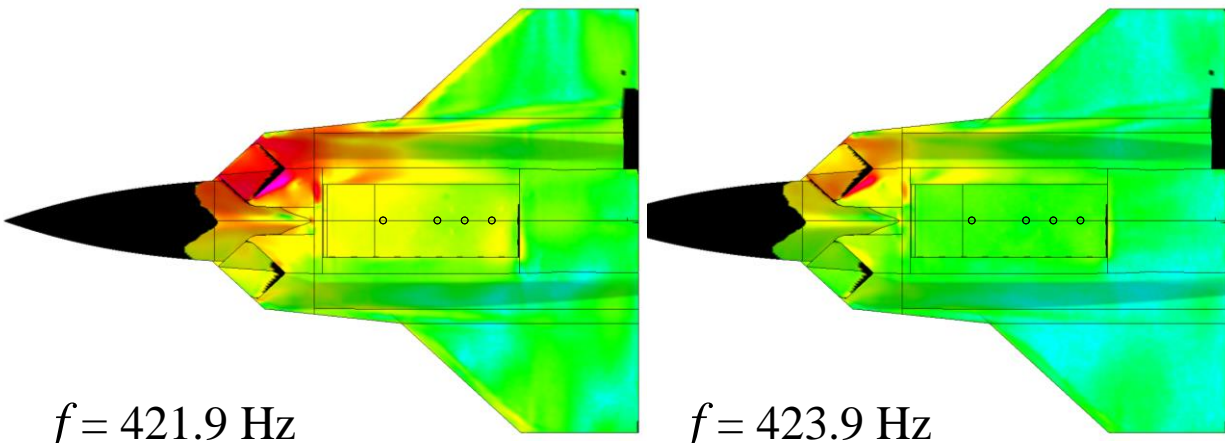
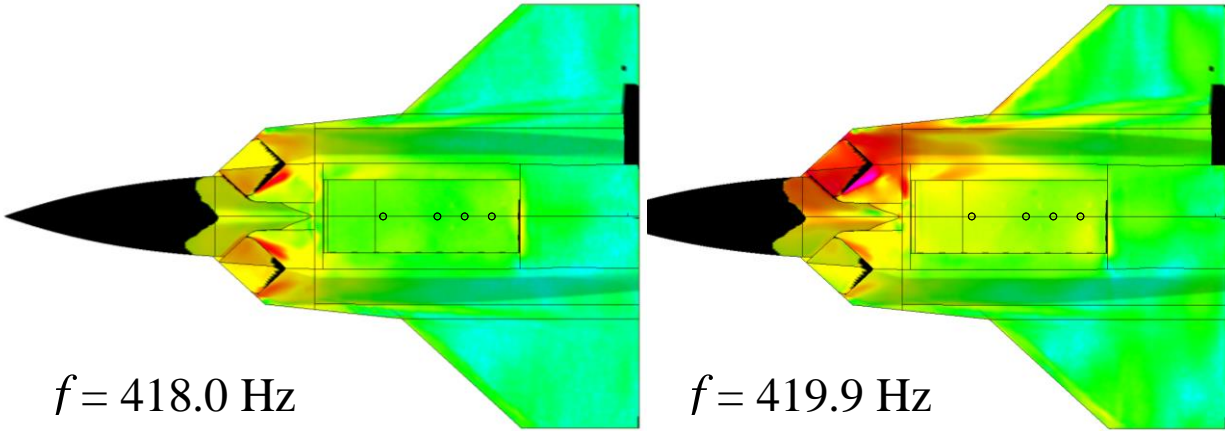


$f = 231.4 \text{ Hz}$

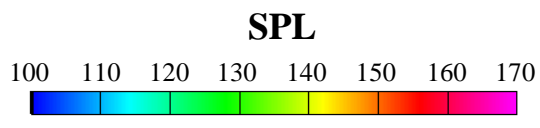
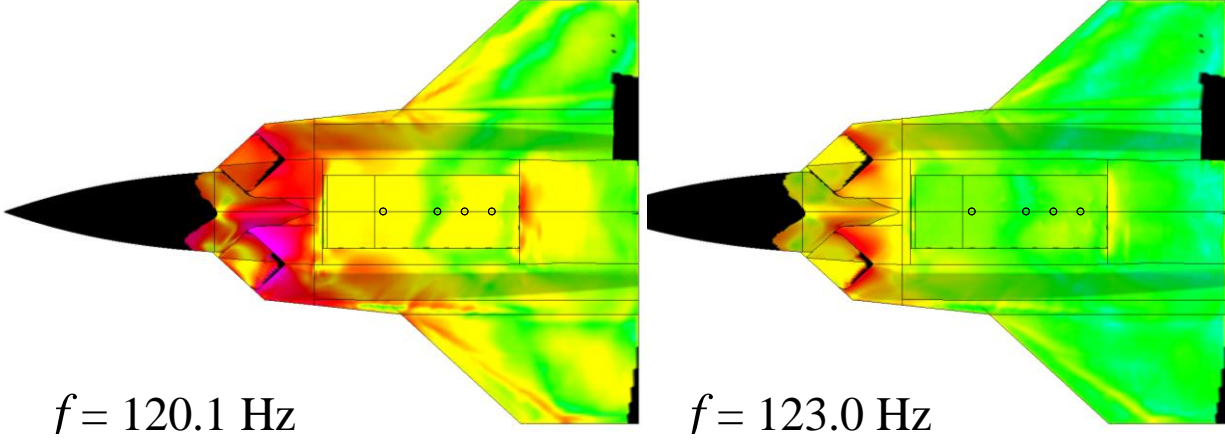
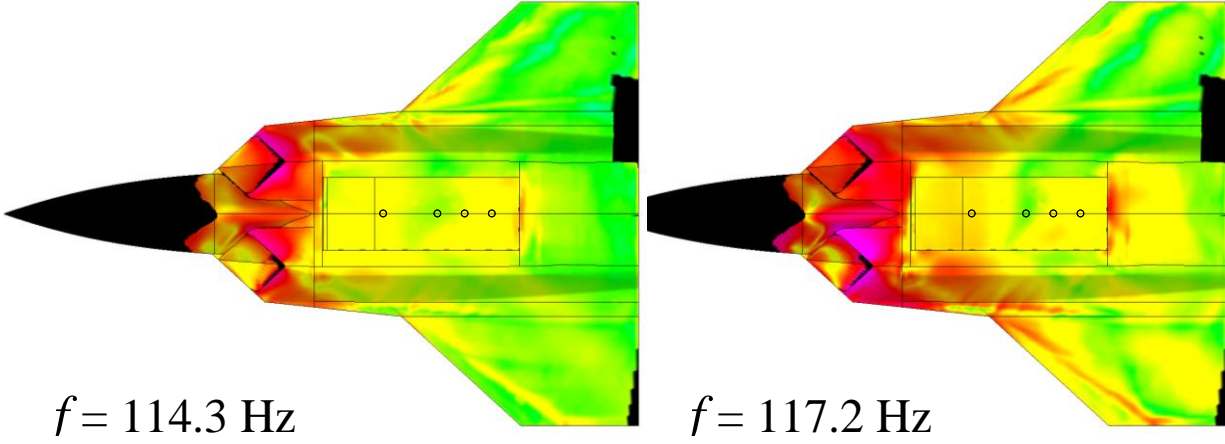
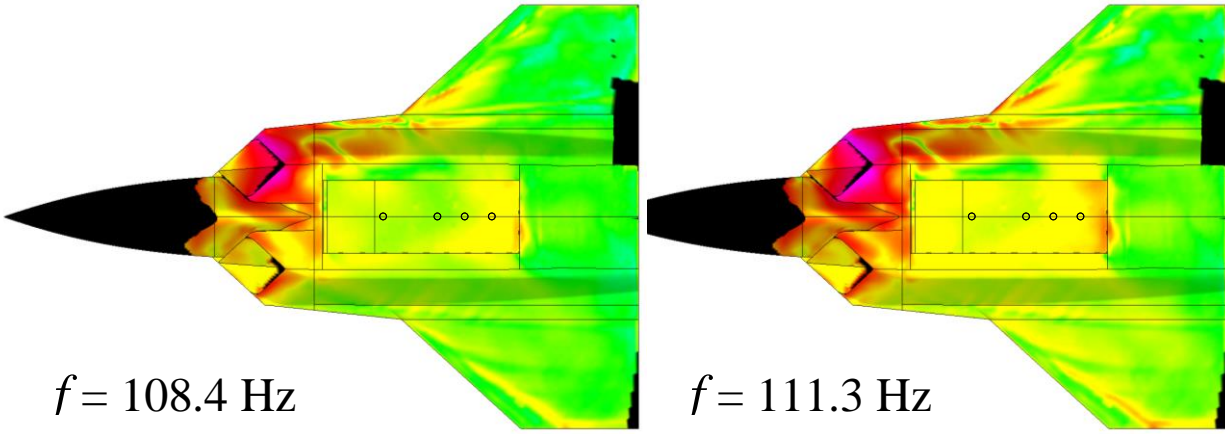
**b. Alpha 0 deg, Beta 0 deg.  
Figure 15. Concluded.**



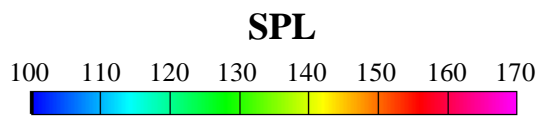
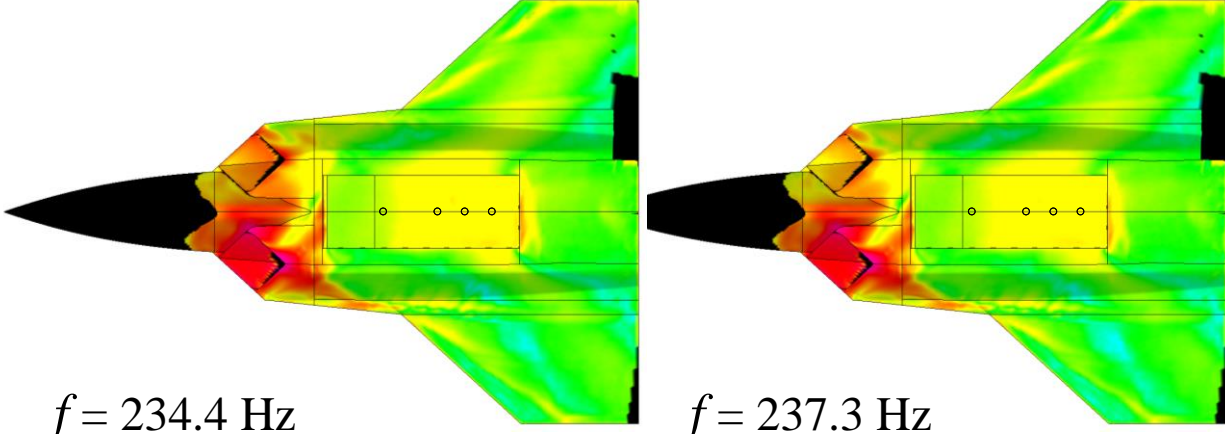
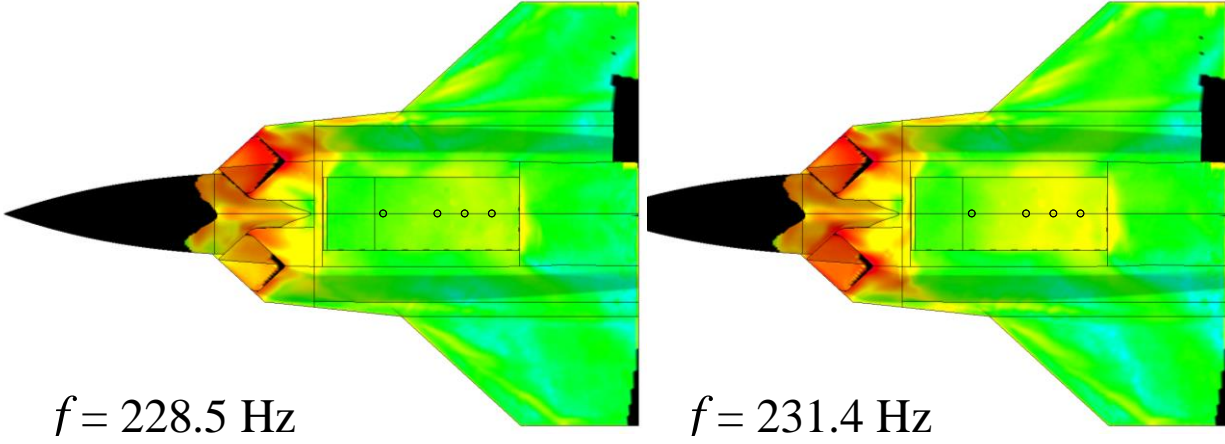
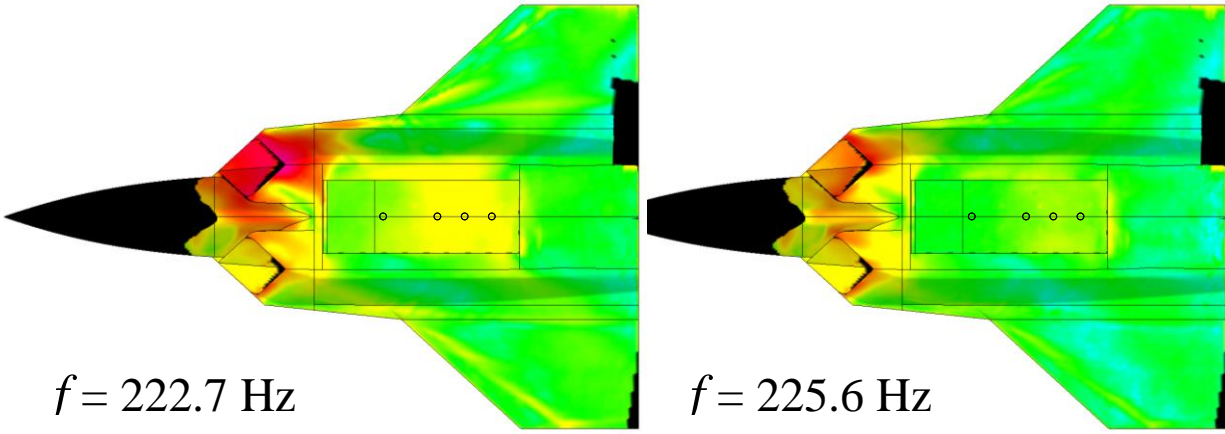
**a. First Peak, Alpha 0 deg, Beta 2 deg.**  
**Figure 16. Beta Effects, Mach 0.9, 100% Blocked.**



**b. Second Peak, Alpha 0 deg, Beta 2 deg.  
Figure 16. Concluded.**



**a. First Peak, Alpha -2 deg, Beta 2 deg.**  
**Figure 17. Beta Effects, Mach 1.3, 100% Blocked.**



**b. Second Peak, Alpha -2 deg, Beta 2 deg.  
Figure 17. Concluded.**

The POD technique, first applied to the analysis of turbulent flows by Lumley (Ref. 19), seeks to represent a high-dimensional pressure field with a low-dimensional model, characterized by the summation of mode shapes, or basis functions:

$$p(x, t) = \sum a_n(t) \varphi_n(x) \quad (6)$$

In Eq. 6,  $x$  represents a spatial coordinate and  $t$  a time coordinate. The pressure,  $p$ , is approximated by the summation of the product of a time constant,  $a_n$ , and a spatial POD mode,  $\varphi_n$  for a discrete set of data. The modes are orthogonal and are ordered according to turbulent kinetic energy. For modal decomposition, the “snapshot” method by Sirovich (Refs. 20 and 21) is used, having obtained a set of  $N$  spatial- and time-resolved data for regions where the model was painted. For each instant in time, a column vector of the fluctuating pressure at  $M$  grid points is organized, which collectively form an  $M \times N$  matrix,  $U$  (Eq. 7). A correlation matrix is created by multiplying the  $U$  matrix with its transpose (Eq. 8). Then an eigenvalue problem is set up according to Eq. 9, where  $A^i$  is the matrix of eigenvectors and  $\lambda^i$  are the eigenvalues. The solution is organized from largest to smallest eigenvalue, with  $\lambda^N = 0$ . Finally, the eigenvectors are used to calculate the POD modes according to Eq. 10.

$$u^i = \begin{bmatrix} u_1^i \\ u_2^i \\ u_3^i \\ \vdots \\ u_M^i \end{bmatrix} \quad U = [u^1 \ u^2 \ u^3 \ \dots \ u^N] \quad (7)$$

$$\tilde{C} = U^T U \quad (8)$$

$$\tilde{C} A^i = \lambda^i A^i \quad (9)$$

$$\varphi^i = \frac{\sum_{n=1}^N A_n^i u^n}{\left\| \sum_{n=1}^N A_n^i u^n \right\|} \quad i = 1, \dots, N \quad (10)$$

After being decomposed into  $N$  modes, the instantaneous pressure field can be reconstructed according to Eq. 6, where the time constant,  $a_n$ , can be calculated according to the following equation:

$$a_n(t) = \text{diag}(\sqrt{\lambda_n}) A_n^T \quad (11)$$

Typically, the predominant flow features are found in the first few POD modes. It is important to determine how many modes are relevant for analysis and how many modes should be used for reconstructing pressure fields, which will be addressed.

Two example cases, Mach 1.3 for inlets 100% open and blocked, are presented to demonstrate the identification of coherent structures from POD modal analysis. The modal analysis was performed on 3,000 of the 4,110 images acquired. The mean flow, normalized energy of each mode, cumulative energy sum, and several important POD modes are presented in Fig. 18.

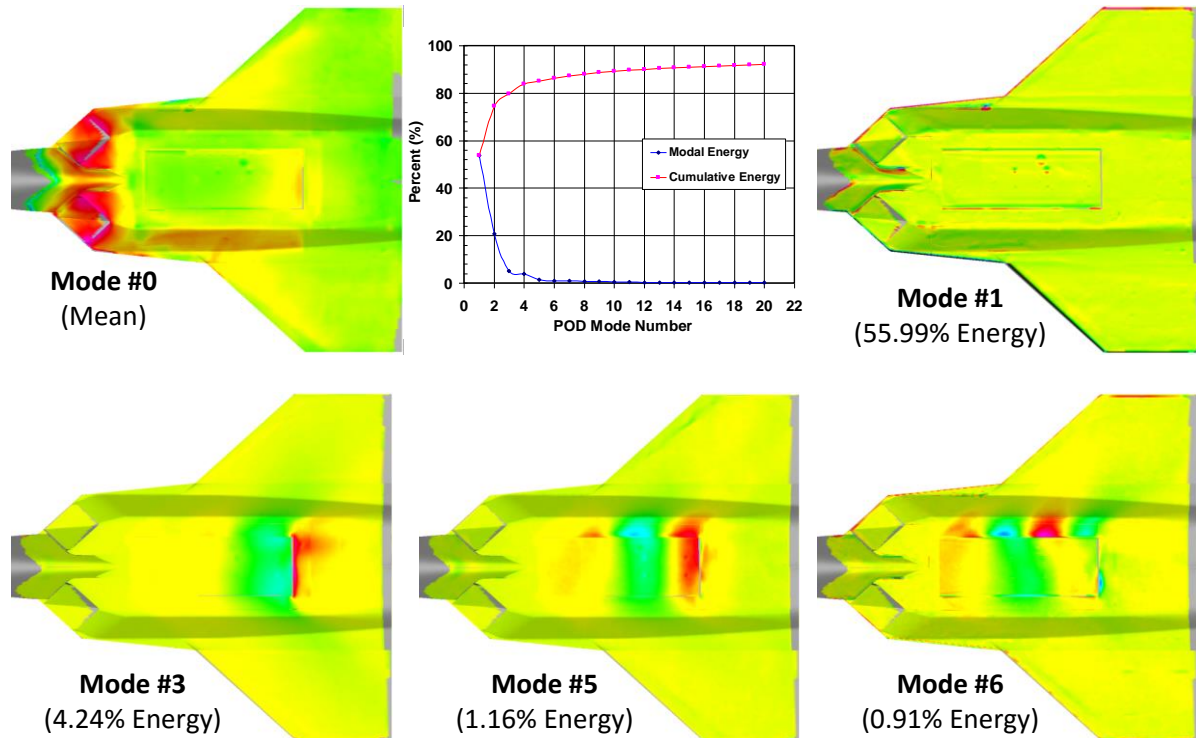


**Figure 18. POD Results, Mach 1.3, Alpha 0 deg, Beta 0 deg, 100% Open.**

The energy breakdown indicates that the first 10 modes are the most significant. The individual contribution of each mode drops off very quickly. The first mode would appear to be extremely significant, comprising 56% of the total energy. However, as depicted in Fig. 18, there are no interesting flow features. Investigation revealed that either model or camera movement generated false pressure fluctuations at low frequencies. This is revealed as a registration error with strong gradients near model edges. Because these pressure patterns occur in every image, the POD analysis identifies it as a flow feature. This served as a confirmation of analysis performed on registration target movement that identified the same frequencies computed from the FFT of target displacement. Modes 2 and 4 had similar characteristics as mode 1. The distribution of energy at Modes 3, 5, and 6 illustrate the interesting patterns revealed by the POD analysis, which was confirmed by analysis done by Rona et al (Ref. 22). For comparison, the SPL distribution at the same condition is presented in Fig. 19. The increased detail is evident when comparing the POD results with the SPL distribution, however, interpreting the POD results is more difficult because the information is more qualitative than quantitative.

The time constant,  $a_n$  (Eq. 11), can be analyzed to understand the frequency content of each POD mode. As an example, the FFT at location D10 was calculated for each of the modes in Fig. 18. The time history of  $a_n$  for each mode and corresponding FFT are presented in Fig. 20. There is a clear difference in the time history of the first mode, associated with an image registration error due to movement of the system, which has a dominant frequency of 5.87 Hz and a secondary peak at 49.9 Hz. Mode 3 has dominant frequencies of 426 Hz and 916 Hz, which correspond closely with the first two Rossiter tones. Mode 5 has dominant frequencies of 417 Hz and 916 Hz; Mode 6 has a dominant frequency of 913 Hz. The frequency response of the first 10 modes is superimposed in Fig. 21, illustrating the contribution of each. The 5.87 Hz component is primarily contained in the first two modes; however, modes 1 and 3 both contain significant content around 50 Hz.

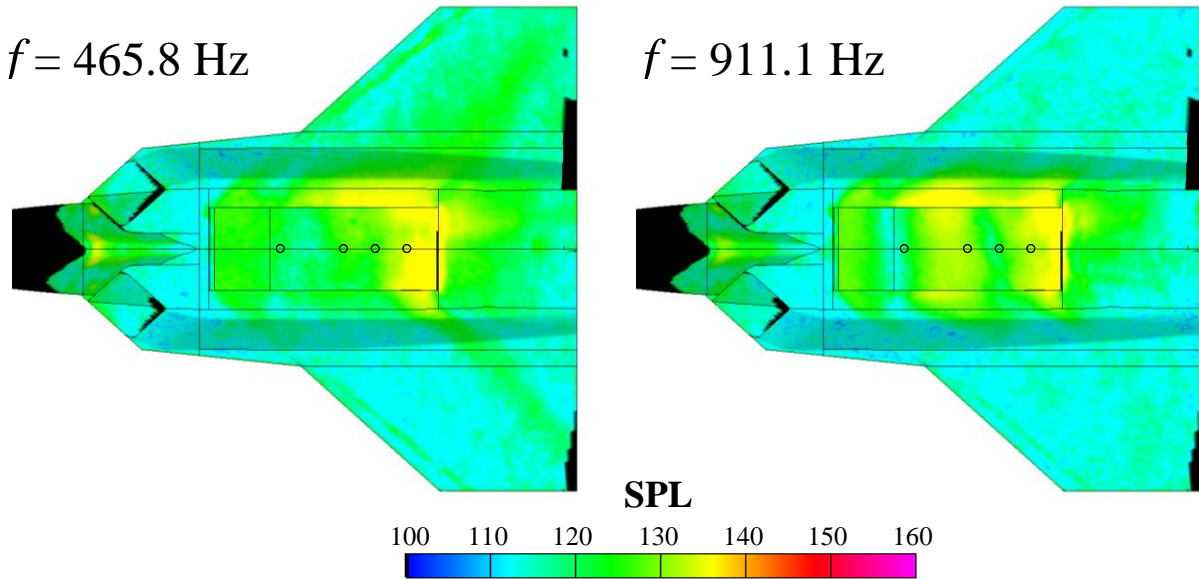


**Figure 19. SPL Distribution, Mach 1.3, Alpha 0 deg, Beta 0 deg, 100% Open.**

An approach was taken to filter the effects of the low frequency movement of the system by reconstructing the pressure field while leaving out the POD modes that contain spurious information. Equations 10 through 15 describe the reconstruction. Typically, a minimal number of POD modes are used to represent the high order system. To determine this number, a frame of the 3D pressure field was randomly chosen from the entire data set and a reconstruction was performed using an increasing number of POD modes (e.g. using one, then one and two, then one, two, and three, etc.), up to 1000 modes. A correlation coefficient was then calculated for each reconstruction compared with the selected frame. Without any smoothing of the original data, the correlation coefficient reaches a maximum of 0.988. If as many modes as there are frames were used, a perfect correlation would be achieved. A sum of 100 modes resulted in a correlation coefficient of 0.963, which was considered sufficient to model the system.

Another correlation was calculated between the first POD mode and 99 successive POD modes. Modes 2, 4, and 9 had the highest correlation and were visually inspected to see that they resembled Mode 1. The PSP pressure field was reconstructed, leaving out these POD modes, and the filtered PSD calculated. The PSD at location D10 for the Kulite<sup>®</sup> data and the original, reconstructed, and reconstructed-filtered PSP data are presented in Fig. 22. The reconstruction compares favorably with the original PSP data, albeit less noisy. There is no significant difference between the reconstructed and reconstructed-filtered PSP data except for attenuation of the lower frequency peaks that were filtered by removing modes. There remains a small offset between the Kulite<sup>®</sup> and PSP at frequencies above 500 Hz, though the important tones match.

The POD results for the 100% blocked configuration are presented in Fig. 23. Again, the first several POD modes contain the majority of the energy. It is interesting to note that no registration errors from model/camera movement appear in the lowest mode numbers. The first indication of possible model/camera movement is mode 8 and was not deemed significant enough to require elimination and reconstruction.

The main flow features are flow separation and vortex shedding around the bottom of the inlet lip. Vortices are again present near the leading edge of the wings, such as in Mode 2. There are occasions where Rossiter tones are created, however, the majority of the flow field is dominated by the vortex shedding from the inlet, which possibly stabilizes the shear layer over the cavity such that it doesn't interact with the trailing edge of the cavity to regularly create pressure waves inside the cavity. The time history of  $a_n(t)$  for each mode and corresponding FFT are presented in Fig. 24. All four modes contain a fundamental frequency of 117Hz and two to four harmonics. In Mode 4, the second harmonic is the dominant frequency.

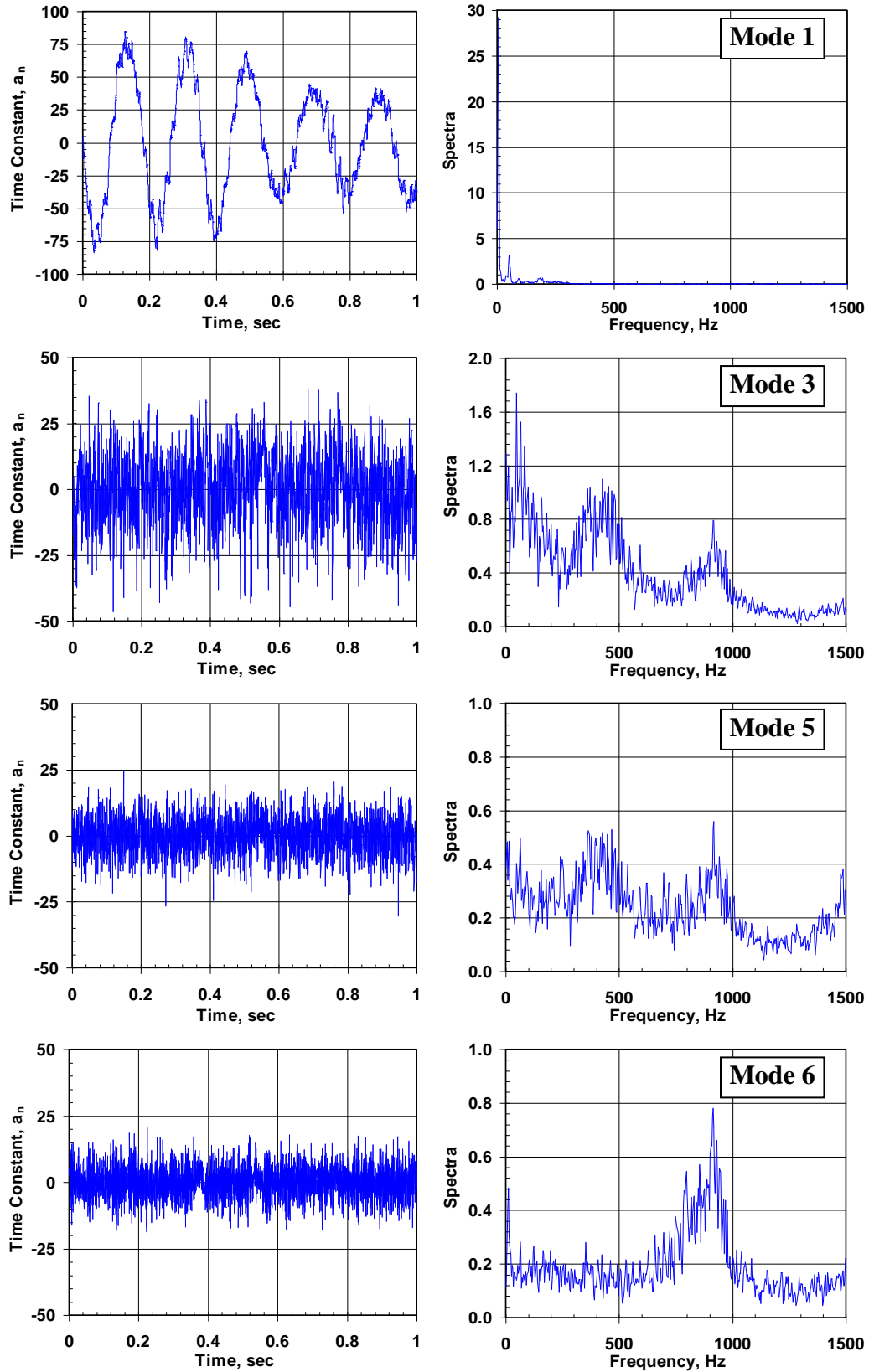


Figure 20. Time History and Frequency Content of the Time Constant, 100% Open.

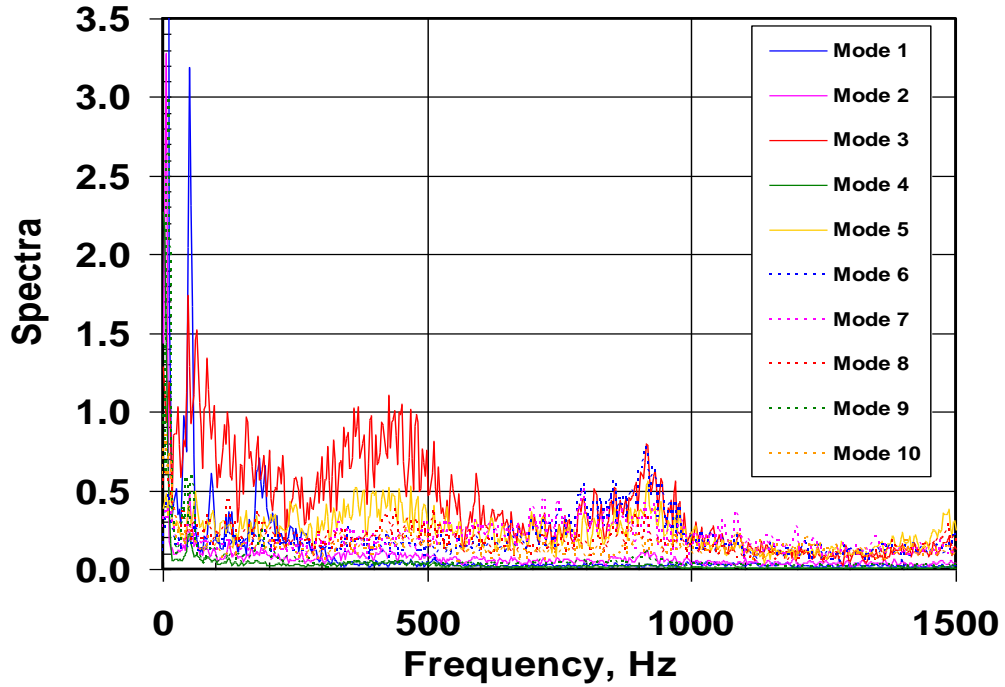


Figure 21. Frequency content of the first 10 POD modes, 100% Open.

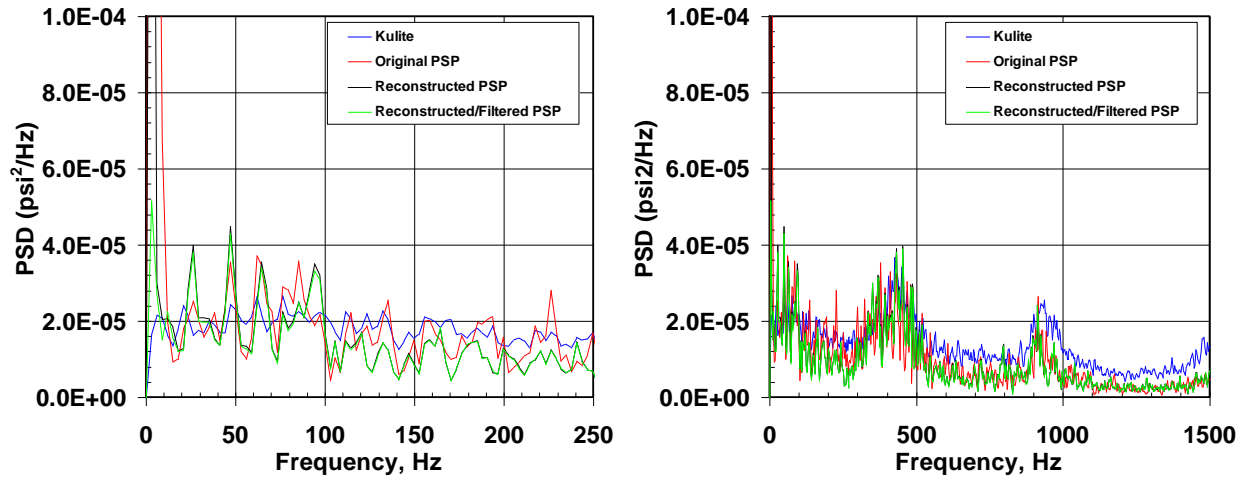
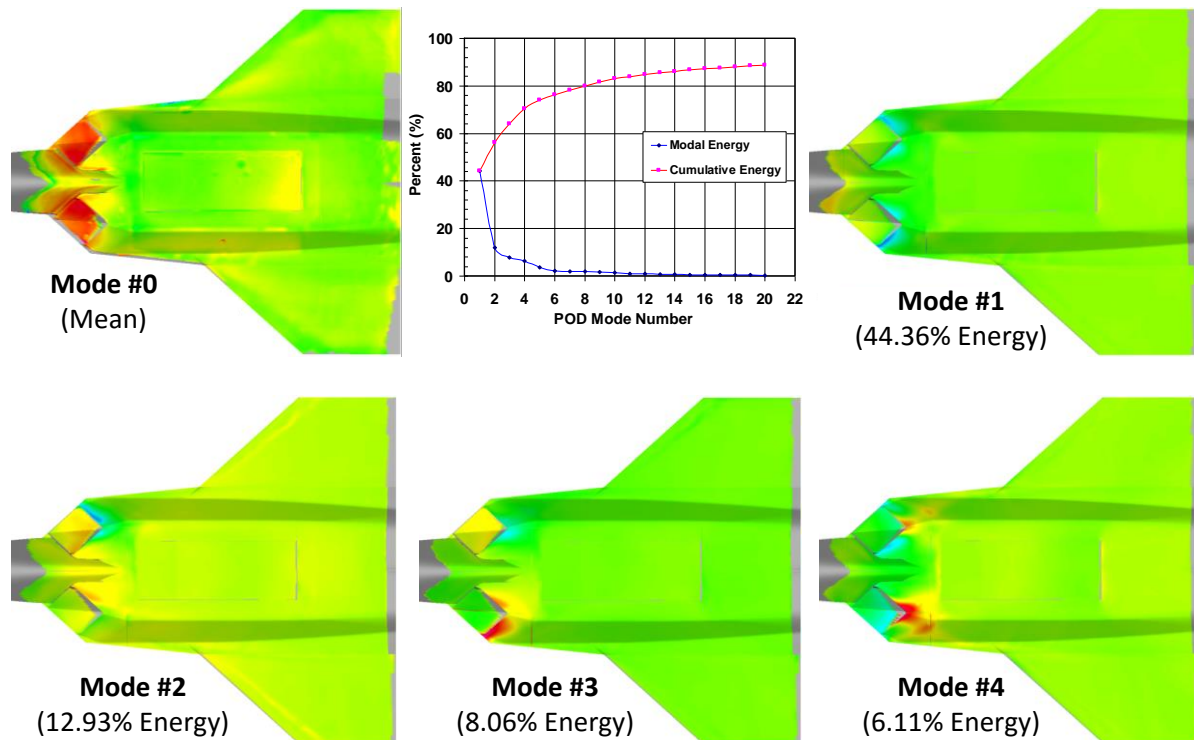


Figure 22. PSD Comparison of Original and POD Reconstructed PSP Data.



**Figure 23. POD Results, Mach 1.3, Alpha 0 deg, Beta 0 deg, 100% Blocked.**

## V. Summary

The use of dynamic PSP on a generic weapons bay model was demonstrated in the AEDC PWT 16T. The PSP data were compared to and validated by dynamic pressure transducers installed in the bay. Proper orthogonal decomposition was performed on the PSP data to identify relevant flow structures. Some conclusions and observations from the test are as follows:

- The power spectral density content from the dynamic PSP compared well with that from dynamic pressure transducers. The peak frequencies matched extremely well while their magnitude comparison varied from good to excellent. The difference may be the result of non-linear gain response of the paint with frequency. An in-depth analysis of the PSP frequency response (gain vs. frequency) is in the planning stage at ISSI. The evaluation will use a new test chamber that can provide significant pressure magnitude fluctuations at different absolute pressure levels.
- The download speeds were slow during the demonstration test, resulting in limited record lengths. AEDC is working on the data acquisition software to speed up the data download from the cameras over the 10Gb Ethernet. As illustrated in the limited long record length data points, the record length of the PSP data needs to be longer so more averaging can be applied and reduce PSP noise.
- The true advantage of dynamic PSP is demonstrated in the full surface SPL distributions. The ability to examine the SPL across the model surface at a selected frequency has never been available with the level of detail PSP provides. Wave cancellation, vortex shedding and other unique dynamic flow features are easily discernable from the PSP. The data acquired from the two cameras during the test are equivalent to more than 250,000 Kulite® transducers.

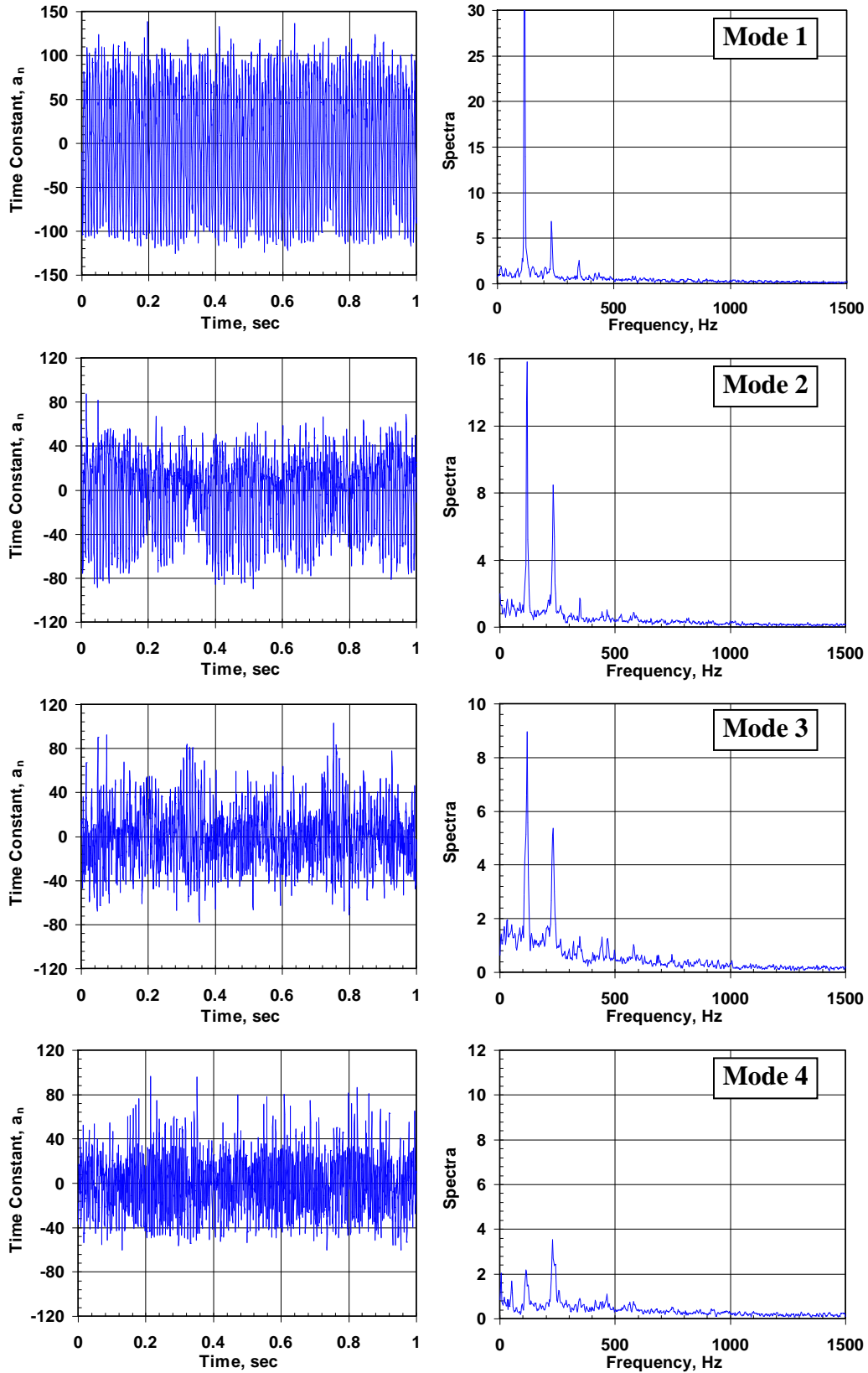


Figure 24. Time History and Frequency Content of the Time Constant, 100% Blocked.

- Analysis using POD was performed on the dynamic PSP data to visualize the dominant flow structures. The POD results identified several modes related to model/camera motion with low frequency content. These results agreed with analysis of registration target movement during acquisition and the low frequencies measured. One unique feature of POD is that of data reconstruction. The modes identified and related to model motion could be left out of data reconstruction which could then be used to calculate filtered PSD data. This process requires considerable computational effort and was not performed on the entire data set. The POD results identified additional (but similar to SPL distribution) flow patterns that dominated the dynamic flow/frequency content.

The results of the test demonstrate the ability to measure dynamic pressure fluctuations in one of the largest transonic wind tunnels in the world. While this test had limited coverage of the test article, AEDC is in the process of developing a full-coverage dynamic PSP capability for 16T. The new system will have 8 cameras distributed around the test cart like the steady-state PSP system.

### **Acknowledgments**

The authors would like to thank Dr. Wim Ruyten of Euclidian Optics, Inc. for developing new image processing capabilities required for this test. Also, thanks to Zach Lowry, private consultant, for developing new data acquisition software and improvement of 10Gb communication for the high speed cameras.

## References

- <sup>1</sup>Sellers, M. E. and Brill, J. A. "Demonstration of a Pressure Sensitive Paint in the AEDC 16-ft Transonic Wind Tunnel Using the TST Model" AIAA Paper 94-2481, 18<sup>th</sup> AIAA Aerospace Ground Testing Conference, Colorado Springs, CO, June 1994.
- <sup>2</sup>Sellers, M. E. "Demonstrations of a Pressure Sensitive Paint Data System in the AEDC Propulsion Wind Tunnel 16T." AEDC-TR-95-8, October 1995.
- <sup>3</sup>Sellers, M. E. "Demonstration Comparison of an AEDC and a Russian Developed Pressure Sensitive Paint in the AEDC Propulsion Wind Tunnel 16T." AEDC-TR-95-88, December 1995.
- <sup>4</sup>Sellers, M. E. "Pressure Sensitive Paint Data on the Transonic Technology Wing Demonstrator (TST) in the AEDC Propulsion Wind Tunnel 16T." AEDC-TR-98-3, June 1998.
- <sup>5</sup>Sellers, M. E. "Application of Pressure Sensitive Paint for Determining Aerodynamic Loads on a Scale Model of the F-16C." AIAA Paper 2000-2528, 21<sup>st</sup> AIAA Aerodynamic Measurement Technology and Ground Testing Conference, Denver, CO, June 2000.
- <sup>6</sup>Sellers, M. E. "Advances in AEDC's Lifetime Pressure-Sensitive Paint Program." AIAA Paper 2005-7638, U.S. Air Force T&E Days, Nashville, TN, December 2005.
- <sup>7</sup>Sellers, M. E. "AEDC's Portable Pressure-Sensitive Paint Data Acquisition System." AIAA Paper 2007-1606, U.S. Air Force T&E Days, Destin, FL, February 2007.
- <sup>8</sup>Sellers, M. E. "Validation of Integrated Panel Loads on a Fighter Aircraft Model Using Pressure-Sensitive Paint at AEDC." AEDC-TMR-08-T2, January 2008.
- <sup>9</sup>Sellers, M. E. "Pressure-Sensitive Paint Data on the Facility Aerodynamics Validation and Research (FAVOR) Model at AEDC." AEDC-TR-09-F-34, December 2009.
- <sup>10</sup>Flaherty, W., Reedy, T. M., Elliot, G. S., Austin, J. M., Schmit, R. F., Crafton, J., "Investigation of Cavity Flow Using Fast-Response Pressure Sensitive Paint," AIAA Paper 2013-0678, 51<sup>st</sup> AIAA Aerospace Sciences Meeting, Grapevine, TX, January 2015.
- <sup>11</sup>Gregory, J. W., Asai, K., Kameda, M., Liu, T., and Sullivan, J. P. "A Review of Pressure-Sensitive Paint for High Speed and Unsteady Aerodynamics," Proceedings of the Institution of Mechanical Engineers, Part G, Journal of Aerospace Engineering, Vol. 222, No. 2, pp. 249-290, (2008).
- <sup>12</sup>Bell, J. H. and McLachlan, B.G. "Image Registration for Luminescent Paint Sensors." AIAA Paper 93-0178, 31<sup>st</sup> Aerospace Sciences Meeting, Reno, NV, January 1993.
- <sup>13</sup>Ruyten, W. M. "Automatic Image Registration for Optical Techniques in Aerodynamic Test Facilities." AIAA Paper 2004-2400, 24<sup>th</sup> AIAA Aerodynamic Measurement Technology and Ground Testing Conference, Portland, OR, June 28-July 1, 2004.
- <sup>14</sup>Rossiter, J., "Wind Tunnel Experiments on the Flow Over Rectangular Cavities at Subsonic and Transonic Speeds," Ministry of Aviation, Aeronautical Research Council, RM3438.
- <sup>15</sup>Tracy, M. B., Plentovich, E. B., and Chu, Julio, "Measurements of Fluctuating Pressure in a Rectangular Cavity in Transonic Flow at High Reynolds Numbers", NASA Technical Memorandum 4363, 1992.
- <sup>16</sup>Berkooz, G., Holmes, P., and Lumley, J., "The Proper Orthogonal Decomposition in the Analysis of Turbulent Flows", Annu. Rev. Fluid Mech., 1993, 25: 539-75.
- <sup>17</sup>Wang, H., Gao, Q., and Wang, J., "Proper Orthogonal Decomposition Based Outlier Correction for PIV Data," 17<sup>th</sup> Int'l Symp. on Appl. of Laser Techniques for Fluid Mech., Lisbon Portugal, 7-10 July 2014.
- <sup>18</sup>Lumley, J., "The Structure of Inhomogeneous Turbulent Flows," Atmospheric Turbulence and Radio Wave Propagation, Nauka Moscow, pp. 166-178.
- <sup>19</sup>Sirovich, L., "Turbulence and the Dynamics of Coherent Structures. Part I: Coherent Structures," Quart. Appl. Math., 45(3):561-571, 1987.
- <sup>20</sup>Meyer, K., Cavar, D., and Pedersen, J., "POD as a Tool for Comparison of PIV and LES Data," 7<sup>th</sup> Int'l Symp. on Particle Image Vel., Rome Italy, 11-4 Sep 2007.
- <sup>21</sup>Rona, A., and Brooksbank, E., "POD Analysis of Cavity Flow Instability," 41<sup>st</sup> AIAA Aerospace Sciences Meeting, AIAA 2003-178, Reno NV, 6-9 Jan. 2003.